ตัวเร่งปฏิกิริยาออกซิเดชันแบบจำเพาะของสารประกอบไทออลที่มีสมบัติแม่เหล็กและกระจายตัวในน้ำได้จากเมทัลเฟอไรต์

นางสาวหฤทัย คงเจริญ

วิทยานิพนธ์นี้เป็นส่วนหนึ่งของการศึกษาตามหลักสูตรปริญญาวิทยาศาสตรมหาบัณฑิต
สาขาวิชาเคมี ภาควิชาเคมี
คณะวิทยาศาสตร์ จุฬาลงกรณ์มหาวิทยาลัย
ปีการศึกษา 2559

WATER-DISPERSIBLE MAGNETIC CATALYSTS BASED ON METAL FERRITE FOR SELECTIVE OXIDATION OF THIOLS

Miss Haruethai Kongcharoen

A Thesis Submitted in Partial Fulfillment of the Requirements
for the Degree of Master of Science Program in Chemistry
Department of Chemistry
Faculty of Science
Chulalongkorn University
Academic Year 2016

Thesis Title	WATER-DISPERSIBLE MAGNETIC CATALYSTS BASED ON METAL FERRITE FOR SELECTIVE OXIDATION OF THIOLS
By	Miss Haruethai Kongcharoen
Field of Study	Chemistry
Thesis Advisor	Numpon Insin, Ph.D.
Thesis Co-Advisor	Associate Professor Sumrit Wacharasindhu, Ph.D.

Accepted by the Faculty of Science, Chulalongkorn University in Partial Fulfillment of the Requirements for the Master's Degree

.....Dean of the Faculty of Science
(Associate Professor Polkit Sangvanich, Ph.D.)

THESIS COMMITTEE

.....Chairman
(Associate Professor Vudhichai Parasuk, Ph.D.)

.....Thesis Advisor
(Numpon Insin, Ph.D.)

.....Thesis Co-Advisor
(Associate Professor Sumrit Wacharasindhu, Ph.D.)

.....Examiner
(Nipaka Sukpirom, Ph.D.)

.....External Examiner
(Samerkhae Jongthammanurak, Ph.D.)

หฤทัย คงเจริญ : ตัวเร่งปฏิกิริยาออกซิเดชันแบบจำเพาะของสารประกอบไทออลที่มีสมบัติแม่เหล็กและกระจายตัวในน้ำได้จากเมทัลเฟอไรต์ (WATER-DISPERSIBLE MAGNETIC CATALYSTS BASED ON METAL FERRITE FOR SELECTIVE OXIDATION OF THIOLS) อ.ที่ปรึกษาวิทยานิพนธ์หลัก: ดร.นำพล อินสิน, อ.ที่ปรึกษาวิทยานิพนธ์ร่วม: รศ. ดร.สัมฤทธิ์ วัชรสินธุ์, 56 หน้า.

ตัวเร่งปฏิกิริยาแม่เหล็กวิวิธพันธุ์เชิงแสงซึ่งจัดว่าเป็น ตัวเร่งปฏิกิริยาอเนกประสงค์ ซึ่งได้รับความสนใจอย่างมากในการนำไปประยุกต์ใช้ในด้านต่างๆ และสามารถใช้ซ้ำได้โดยใช้แรงแม่เหล็กในการแยกตัวเร่งออกจากปฏิกิริยาได้อย่างมีประสิทธิภาพ อนุภาคแม่เหล็กนาโนเฟอร์ไรต์สามารถสังเคราะห์ด้วยวิธีสลายตัวทางความร้อน (thermal decomposition) ของเหล็ก (III) โอเลเอต (Iron (III) oleate) ในตัวทำละลาย 1-ออกตะเดคซีน (1-octadecene) และกรดโอเลอิค (oleic acid) ซึ่งเป็นวิธีที่สังเคราะห์ได้ง่าย ค่าใช้จ่ายไม่สูง และได้อนุภาคแม่เหล็กเฟอร์ไรต์ในปริมาณมาก

สำหรับงานนี้อนุภาคแม่เหล็กนาโนเฟอร์ไรต์ถูกสังเคราะห์ขึ้นโดยเปลี่ยนชนิดของโลหะในโครงสร้างแม่เหล็กนาโนเฟอร์ไรต์ (MFe_2O_4) เมื่อ M คือ แมกนีเซียม (Mg), เหล็ก (Fe), โคบอลต์ (Co), นิกเกิล (Ni), ทองแดง (Cu) และ แมงกานีส (Mn) ที่มีเส้นผ่านศูนย์กลาง 6-13 นาโนเมตร สามารถตรวจพิสูจน์เอกลักษณ์และยืนยันอนุภาคที่สังเคราะห์ขึ้นด้วย เครื่องจุลทรรศน์อิเล็คตรอนแบบส่องผ่าน (Transmission Electron Microscope, TEM), เครื่องจุลทรรศน์อิเล็คตรอนส่องกราดที่มีเครื่องตรวจวัดธาตุองค์ประกอบ (Scanning Electron Microscope-Energy Dispersive X-ray, SEM-EDX) และเครื่องวิเคราะห์การเลี้ยวเบนรังสีเอกซ์ (X-ray Diffractometer) นอกจากนี้คอมพอสิตระหว่างแม่เหล็กเฟอร์ไรต์กับไทเทเนีย ($MgFe_2O_4$@TiO_2 composites) ถูกสังเคราะห์ขึ้นโดยวิธีรีเวิร์สไมโครอิมัลชัน (reverse microemulsion) เพื่อนำไปใช้ในการเร่งปฏิกิริยาออกซิเดชันแบบจำเพาะของสารประกอบไทออล อย่างไรก็ตามภายใต้สภาวะไร้แสง $MgFe_2O_4$ ก็สามารถเร่งปฏิกิริยาออกซิเดชันของสารตั้งต้น 4-คลอโรไทโอฟีนอล (4-chlorothiophenol) ได้อย่างสมบูรณ์และไม่แตกต่างจากคอมพอสิตระหว่างแม่เหล็กเฟอร์ไรต์กับไทเทเนียภายในเวลา 1 ชั่วโมง ดังนั้นผู้วิจัยจึงทำการศึกษาประสิทธิภาพในการเร่งปฏิกิริยาของอนุภาคแม่เหล็กนาโนเฟอร์ไรต์ชนิดต่างๆ และพบว่าตัวเร่งปฏิกิริยาวิวิธพันธุ์ที่ดีที่สุดคือ คอปเปอร์เฟอร์ไรต์ ($CuFe_2O_4$) ซึ่งสามารถเร่งปฏิกิริยาในน้ำได้อย่างสมบูรณ์โดยใช้เวลา 2 วัน ภายใต้สภาวะปกติ ณ อุณหภูมิห้อง หลังจากเสร็จสิ้นการเร่งปฏิกิริยาตัวเร่งแม่เหล็กนาโนเฟอร์ไรต์สามารถแยกออกมาได้ด้วยแรงแม่เหล็ก พบว่าตัวเร่งคอปเปอร์เฟอร์ไรต์สามารถใช้ได้อย่างมีประสิทธิภาพสูงสุดถึง 4 ครั้ง แสดงให้เห็นว่าตัวเร่งดังกล่าวมีประสิทธิภาพในการเร่งปฏิกิริยาออกซิเดชันแบบจำเพาะของสารประกอบไทออล อีกทั้งยังมีทั้งสมบัติทางแม่เหล็กในตัวเองอีกด้วย

ภาควิชา เคมี	ลายมือชื่อนิสิต .....
สาขาวิชา เคมี	ลายมือชื่อ อ.ที่ปรึกษาหลัก .....
ปีการศึกษา 2559	ลายมือชื่อ อ.ที่ปรึกษาร่วม .....

5772290523 : MAJOR CHEMISTRY
KEYWORDS: METAL FERRITE NANOPARTICLES / SELECTIVE OXIDATION OF THIOLS / DISULFIDE COMPOUND / 4-CHLOROTHIOPHENOL

HARUETHAI KONGCHAROEN: WATER-DISPERSIBLE MAGNETIC CATALYSTS BASED ON METAL FERRITE FOR SELECTIVE OXIDATION OF THIOLS. ADVISOR: NUMPON INSIN, Ph.D., CO-ADVISOR: ASSOC. PROF. SUMRIT WACHARASINDHU, Ph.D., 56 pp.

Heterogenous magnetic photocatalyst, so-called multifunctional catalyst, has been of an intensive interests for using in many research fields. It can be also reused for several times after catalyzed the reaction by using magnetic field for separation. Magnetic metal-ferrite nanoparticles were synthesized by thermal decomposition method of iron (III) oleate in 1-octadecene in the presence of oleic acid leads to a simple, cost effective synthesis route for large scale monodisperse ferrite nanoparticles.

Herein, Spherical magnetic metal ferrite (MFe_2O_4) with the diameter 6-13 nm, where M represents Mg, Fe, Co, Ni, Cu, and Mn, while maintaining the spinel crystal structure. The as-synthesized metal ferrites nanoparticles were characterized by using TEM, SEM-EDX, and XRD for their composition, size, shape, and structure. Moreover, $MgFe_2O_4@TiO_2$ core-shell structure was created by reverse-microemulsion for using in the selective oxidation of thiols. However, $MgFe_2O_4@TiO_2$ nanocomposites effectively catalyzed the aerobic oxidation of 4-chlorothiophenol under dark condition as well as $MgFe_2O_4$ without TiO_2 shell decoration within an hour reaction time. Therefore, the single metal ferrite with various metal would be interesting to further utilize instead of $MgFe_2O_4@TiO_2$ core-shell structure. Among all of metal ferrite nanoparticles, $CuFe_2O_4$ nanoparticles would be outstanding candidates for using under ambient condition in aqueous solution within 2 day to complete the aerobic oxidation of 4-chlorothiophenol to disulfide products. Magnetic metal ferrites can be magnetically recovered after finishing the reaction and reused up to forth runs without any significantly loss of catalytic activity. Therefore, these magnetic catalysts were effectively used in the selective oxidation of thiols that perform the catalytic property and magnetic property within the same materials.

Department:	Chemistry	Student's Signature	.....
Field of Study:	Chemistry	Advisor's Signature	.....
Academic Year:	2016	Co-Advisor's Signature	.....

ACKNOWLEDGEMENTS

My deep gratitude goes first to Dr. Numpon Insin, who is my thesis advisor, not only expertly guided me through my graduate education to successfully achieve my thesis, provided all of crucial and beneficial information for my thesis and persuaded PhD study, but also shared the excitement of six years' discovery since Bachelor's degree in his laboratory. In addition, his personal generously helped make my time at Chulalongkorn University enjoyable.

Also, I would like to appreciate for worthy comments and counsels from my thesis committee; Associate Professor Dr. Vudhichai Parasuk, Dr. Nipaka Sukpirom, and Dr. Samerkhae Jongthammanurak who is my external committee from National Metal and Materials Technology Center (MTEC). This research would have not been completed without all of their kindness. Moreover, it is my honor to have Associate Professor Dr. Sumrit Watcharasidhu to be my co-advisor, who advised me a versatile knowledge and guided me about the practical technique for organic manipulation.

Furthermore, my appreciation also extends to my colleagues, all of Materials Chemistry and Catalysis Research Unit's members who are always kind and helpful. Particularly, Miss Wishulada Injumpa, Miss Chalatan Saengruengrit, and Miss Padtaraporn Chunhom.

Above ground, I am undoubted to be respectful and value my family, who looks after and supports all of everything in my life and my thesis; moreover, they are the enormous source of my encouragement for driving on my goal, also this research.

Eventually, I would like to thank the scholarship from the Graduate School, Chulalongkorn University to commemorate the 72 anniversary of his Majesty King Bhumibala Aduladeja is gratefully acknowledged for supporting my graduate study. We are also grateful with Department of Chemistry, Faculty of Science, Chulaongkorn University for laboratory facilities and instruments.

CONTENTS

Page

Page

Page

LIST OF TABLES

LIST OF FIGURES

LIST OF SCHEMES

LIST OF ABBREVIATION

M	=	Magnetization
M_R	=	Remanent magnetization
M_S	=	Saturation magnetization
H_c	=	Coercivity
P25	=	Commercial titanium dioxide
MFe_2O_4	=	Magnetic metal-ferrite
M@T	=	Magnesium ferrite@tinanium dioxide
$MFe_2O_4@TiO_2$	=	Magnetic metal-ferrite@titanium dioxide
Fe_3O_4	=	Magnetite
γ-Fe_2O_3	=	Maghemite
α-Fe_2O_3	=	Hematite

CHAPTER I
INTRODUCTION

1.1 Statement of the problem

Nowadays, there are many catalysts that have been used for increasing the rate of oxidation reaction; however, most problematic chemical reactions occurred as stoichiometric amounts of toxic catalysts are traditionally required. The aforementioned problem causes severe environmental impacts and unsafe operational practices. Thus, photocatalysts are promising alternative substances to harvest the products from organic transformation in particular oxidation reactions under very mild condition using light irradiation [1-3] . Titania (TiO_2) is the most widely used photocatalysts for photocatalytic reactions because of its slow charge recombination rate as one of the prominent properties. However, the large band gap (3.0-3.2 eV) [4] of titania enables photocatalysis only under UV irradiation, a region of which contributes only 2-5% in solar spectrum. Moreover, many studies found that reactions using both homogeneous and heterogeneous catalysts are still suffered from the separation of the catalysts from the reaction mixtures, leading to not only the contaminations of heavy metals and organic pollutants to environment, but also decrease in the possibility to reuse catalysts. This work is focusing on conserving the high photocatalytic activity of TiO_2 with the improvement in visible light activation and magnetic separation of the used catalysts by incorporating magnesium ferrite ($MgFe_2O_4$) nanoparticles into titania.

$MgFe_2O_4$ is superparamagnetic semiconductor that could lead to smaller band gap and high magnetic response with high colloidal stability. There have been reports on the catalytic activities of $MgFe_2O_4$ and their related ferrites with similar structure. The capacity of single MFe_2O_4 still can be effectively used through many kinds of organic transformation reactions such as oxidation reaction of alkene, condensation of aldehyde, alkylation, dehydrogenation, etc., [5]. Therefore, the efficiency of various metals of magnetic ferrite (MFe_2O_4) structures as catalyst would be also investigated in this study. The catalytic performance of $MgFe_2O_4/TiO_2$ nanocomposites and MFe_2O_4

nanoparticles will be studied and could hopefully result in a new class of catalysts with high efficiency and ease of use.

1.2 Objectives of research

1.2.1 To synthesize $MgFe_2O_4/TiO_2$ nanocomposites as multifunctional catalysts

1.2.2 To evaluate catalytic activity of $MgFe_2O_4/TiO_2$ nanocomposites using in selective oxidation of thiol compound under ambient condition

1.2.3 To synthesize magnetic nanoparticles of various metal ferrite (MFe_2O_4) and investigate their catalytic activity in aerobic oxidation of thiol

1.3 Scope of this thesis

MFe_2O_4 nanoparticles have been synthesized by thermal decomposition method. Also, the core $MgFe_2O_4$ has been modified with TiO_2 precursor by reverse-microemulsion process as $MgFe_2O_4/TiO_2$ nanocomposites. The nanocomposites were characterized by transmission electron microscope (TEM), scanning electron microscope–energy dispersive x-ray (SEM-EDX), and X-ray diffractometer (XRD). The $MgFe_2O_4/TiO_2$ nanocomposites and metal ferrites will be further investigated for their catalytic performance in selective oxidation of thiol at various conditions including different solvents, varied catalyst amount, and time. The efficiency of this catalyst was estimated by the ratio of integration from nuclear magnetic resonance spectrometer (NMR).

1.4 Expected beneficial outcome

Water-dispersible $MgFe_2O_4/TiO_2$ nanocomposites and MFe_2O_4 nanoparticles will be obtained, and they can be used as efficient multifunctional catalysts in oxidation for organic chemistry reaction.

CHAPTER II

THEORY AND LITERATURE REVIEWS

2.1 Materials

2.1.1 Magnetic properties of materials [6]

Every substance has its own magnetic property. There are 4 types of magnetic properties when the materials contain atoms with unpaired electron on its own as shown in ***Figure 2.1***. Ferromagnetic materials contain aligned atomic magnetic moments all in the same direction and produce large net magnetic moment; therefore, the response of these materials is strongly attractive towards a magnet. Meanwhile, materials having atomic magnetic moments of equal magnitude that are arranged in an anti-parallel fashion and result in no net magnetic moment display antiferromagnetic. Antiferromagnetic materials are weekly attractive from a magnetic field. Moreover, materials will exhibit paramagnetic behavior when thermal energy is adequate for atomic moments to fluctuate randomly. In case of paramagnetic, the response is weakly attractive towards a magnet. On the other hand, materials that possess different strengths of magnetic moments that are arranged in an anti-parallel fashion and produce a net magnetic moment exhibited behavior of ferrimagnetism. Ferrimagnetic materials are strongly attractive towards a magnetic field.

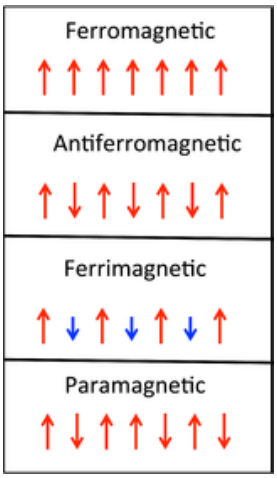

Figure 2.1 *Magnetic moment orientation*

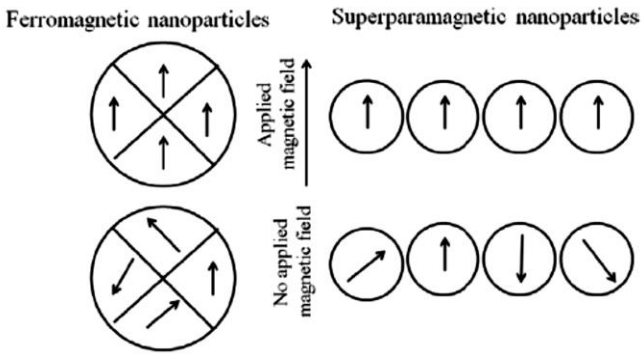

Figure 2.2 *Orientation of magnetic moments of ferromagnetic and superparamagnetic nanoparticles with and without an applied magnetic field* ***[7]***

2.2.2 Magnetic nanoparticles and superparamagnetic properties

Phenomenon of superparamagnetism arises when the size of a particle becomes small enough to exhibit single domain, and the magnetic moment fluctuates in random direction because of thermal activation [8] (***Figure 2.2***). The term superparamagnetism also refers to strong magnetic response with characteristic paramagnetic nature of non-permanent magnetization (***Figure 2.3a***), However, when the magnetic field is applied, the magnetic moment absolutely aligns with the same direction of applied magnetic field (***Figure 2.3c***). The similar response is found in ferromagnetic materials (***Figure 2.3b***).

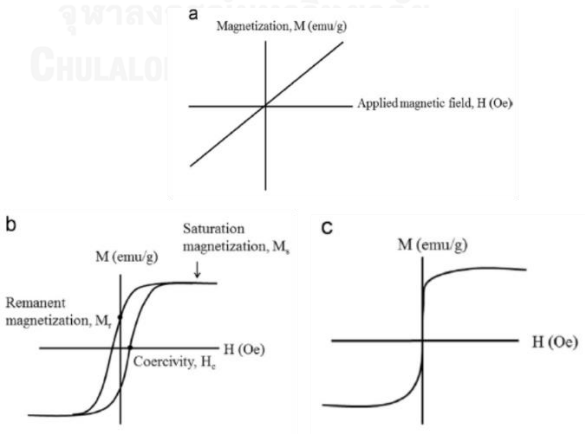

Figure 2.3 *Magnetic responses when applied magnetic field a) paramagnetic, (b) ferromagnetic and (c) superparamagnetic materials*

2.2 Synthesis of magnetic metal ferrite nanoparticles (MNPs)

Monodisperse magnetic nanomaterials have been intensively focused in recent years, due to fundamental scientific interest and technological applications based on the unique physicochemical properties and large–scale applicability in the field of imaging, photonics, nanoelectronics, solid support, sensors, bio-materials, and biomedicine [9-14]. Magnetic nanomaterials have been widely utilized as environmentally benign heterogeneous catalysts in oxidation reaction to address various economic and environmental issues [15-17]. Depending on the chemical identity of M^{2+}, so-called metal ferrites, MFe_2O_4 (where M=Mg, Fe, Co, Ni, Cu, Mn, etc.) or half-metallicity (where M=Fe), may be a promising candidate for high-performance electromagnet in the future [18].

To date, there have been numerous methods to synthesis MFe_2O_4 nanocrystals. These methodologies have been based on hydrothermal [19], solvothermal [20], co-precipitation [21], electrochemical manipulation [22], microemulsion [23], and other solution-based treatments [24] (i.e. sol-gel, polyol, etc.). The tuning of shape, size, and crystallinity can additionally affect the properties of magnetic nanocrystals [25]. Therefore, a simple and cost-effective synthesis route for large-scale production of monodisperse ferrite nanocrystals, with tunability shapes and sizes, would be very attractive for practical applications. However, the obtained products often suffer from particle agglomeration and a broad size distribution. In order to obtain monodisperse nanoparticles, suitable precursor systems that can generate stable monomers in solution are necessary. One of the most successful routes involves thermal decomposition of mixed organic M^{2+} and Fe^{3+} compounds, such as metal carbonyl, metal acetylacetonate, etc. in high boiling point solvents including surfactants such as oleic acid and oleylamine. This procedure results in the formation of monodisperse ferrite nanoparticles with good crystallinity and uniform size as shown in ***Figure 2.4*** [26].

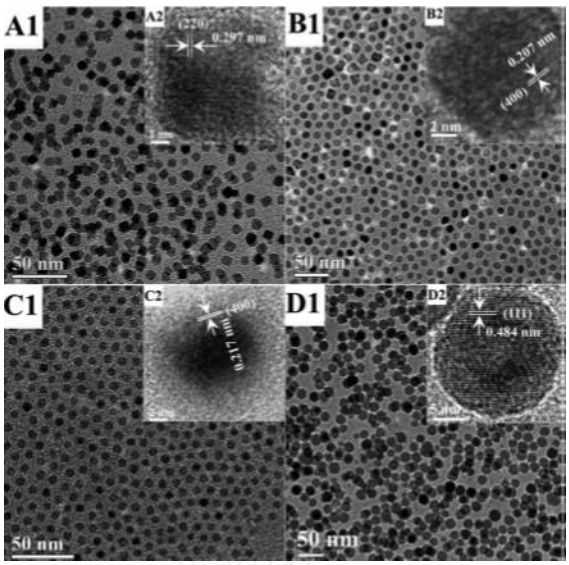

Figure 2.4 *TEM micrographs of MFe_2O_4 nanoparticles: (A1) $CoFe_2O_4$; (B1) $NiFe_2O_4$; (C1) $MnFe_2O_4$; (D1) Fe_3O_4. The corresponding high resolution TEM micrograph of the individual nanoparticles is shown in the inset [26]*

According to the superparamagnetic character of magnetic nanomaterials of ferrite, there are several researches on ferrites in term of dual properties not only as magnetic materials, but also catalysts as discussed in the ***Section 2.3***.

2.3 Catalytic process

2.3.1 Catalytic process

2.3.1.1 Catalysis

Catalysis is the process of decreasing the activation energy to dramatically drive chemical reaction rate because of the presence of catalyst, which does not decay in the catalytic reaction and can be reused effectively. Only small amounts of catalyst are required for highly efficient catalysis.

2.3.1.2 Photocatalysis

Photocatalysis is the activation of a reaction in the presence of photocatalysts. The photocatalytic activity (PCA) depends on the ability of the catalysts to create the separation of electron–hole pairs, which generate free radicals (e.g. hydroxyl radicals: •OH) from oxidation at valence band and superoxide anion from reduction at

conduction band. In the other word •OH and O_2^- are considered as reagents for secondary reactions as shown in ***Figure 2.5***.

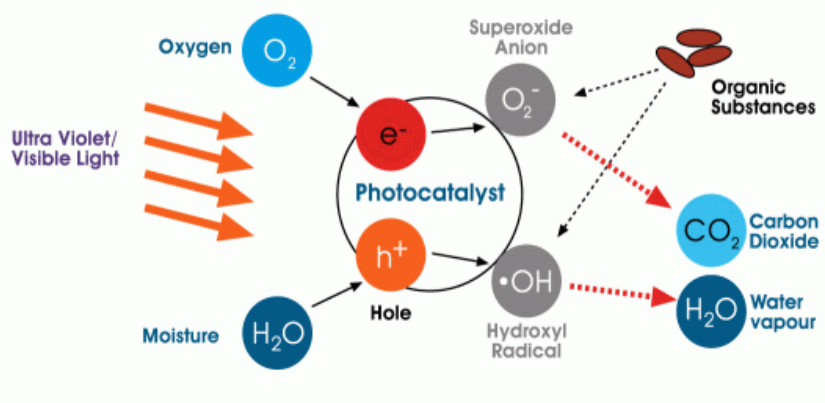

Figure 2.5 *Proposed photocatalytic mechanism [7]*

Electron and hole are produced by photoactivation of the solid **(*Equation 2.1*)**. The excited electron and hole can recombine and release the energy gained from the excitation of the electron as heat ***(Figure 2.6)***.

$$hv + \text{Metal-oxide} \longrightarrow \text{Metal-oxide}\ (h^+ + e^-) \qquad (2.1)$$

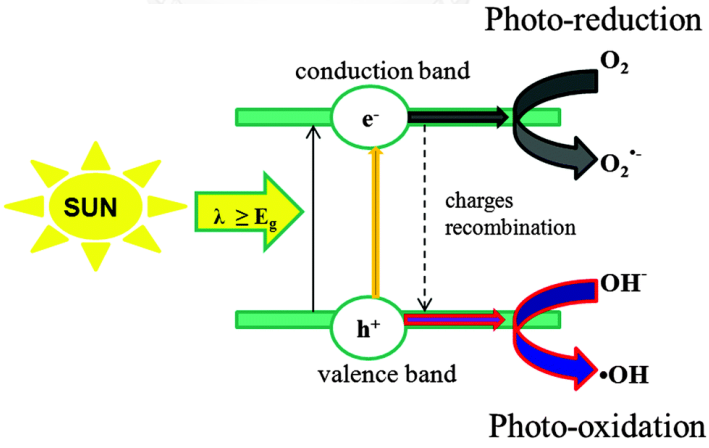

Figure 2.6 *Photocatalytic mechanism of electron and hole separation [27]*

2.3.2 Type of catalyst

2.3.2.1 Homogeneous catalysts

In homogeneous catalysis, the reactants and catalysts coexist in the same phase. For example, ozone and photo-Fenton systems [28] (Fe^{2+} and Fe^{3+}/H_2O_2) are the most commonly used as homogeneous photocatalyst that generates •OH as reactive species.

2.3.2.2 Heterogeneous catalysts

In heterogeneous catalysis, the reactants and catalysts exist in different phases. The catalysts can be utilized in a large variety of reactions: mild and total oxidations, dehydrogenation, hydrogen transfer, water splitting, gaseous and organic pollutant removal, etc. Ones of the most common heterogeneous photocatalysts are transition metal oxides and semiconductors for their distinctive characters. Semiconductors possess a band gap energy region which states between valence band (the highest energy level of electron occupancy) and conduction band (the lowest energy level of electron inoccupancy). When photons with equal or greater energy were absorbed, electrons are excited from the valence band to the conduction band, generating a positive hole in the valence band which are the source of active electron and hole for utilizing in redox reaction.

2.4 Usefulness of the disulfide compounds

Disulfide compounds or organic compounds possessing S-S bonds, have been comprehensively studied in versatile fields such as synthetic intermediates for organic transition [29] and have found widely in pharmaceutical ***(Scheme 2.1)*** [30] and material sciences [31]. Moreover, the formation of S-S bonds plays a significant role for stability and folding the proteins in biological systems [31] as shown in ***Scheme 2.2.***

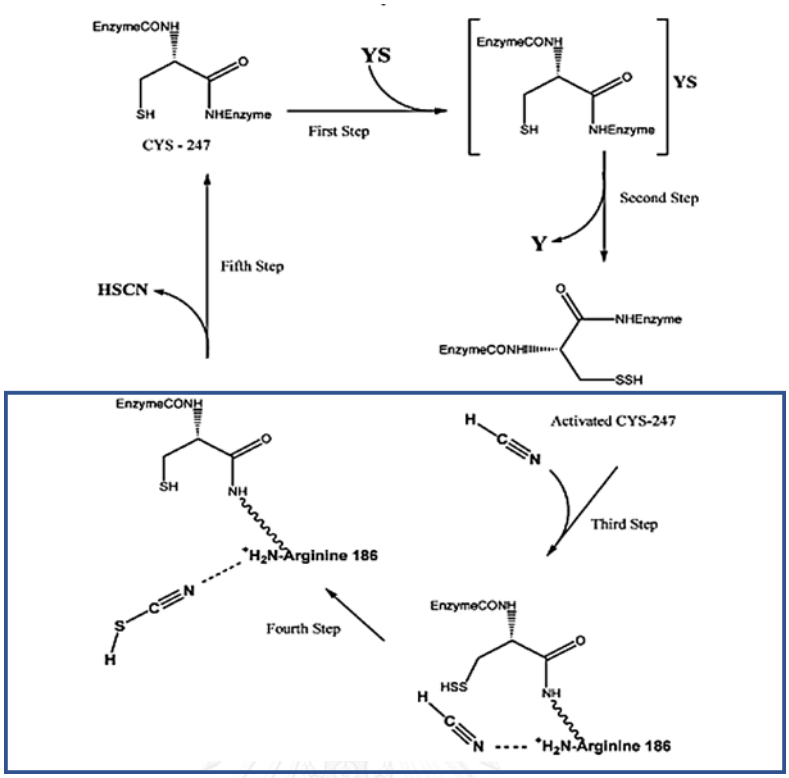

Scheme 2.1 *Mechanism of Rhodanase-Mediated Detoxification of Cyanide [30]*

Additionally, disulfides can be industrially used in the vulcanization process for rubbers and elastomers to reinforce the material properties [32]. In recent studies, It is revealed that oxidized species of disulfide were useful for agro-chemicals [33] as shown in the variety of novel sulfur-based crop pesticides around the world.

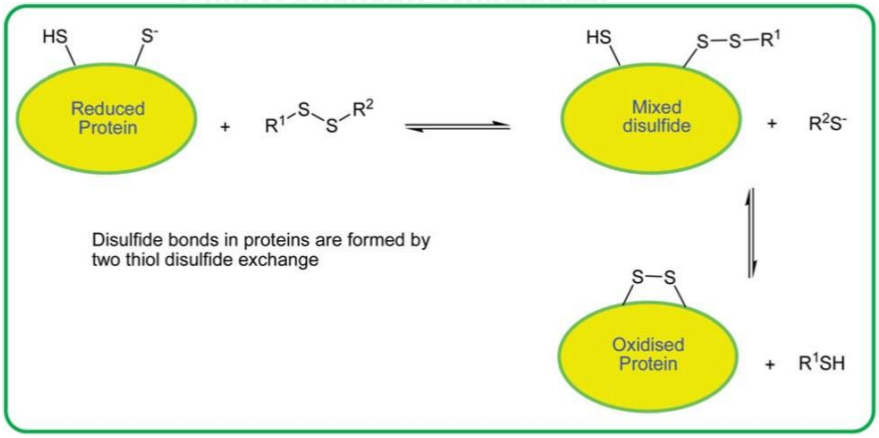

Scheme 2.2 *Role of disulfide bond in protein folding*

2.5 Literature reviews

2.5.1 Catalyst for organic transformation

TiO_2 photocatalyst is versatilely used in many research fields, including self-cleaning surfaces, air and water purification, water splitting, hydrogen production, and photcatalyst for organic transformation [34]. Recently, Lang *et al.* [2, 35] were interested in the photoredox synergistic catalysis of sulfides and amines on the surface of TiO_2 ***(Scheme 2.3-2.5)*** under visible light irradiation for selective oxidation of sulfide to sulfoxide with oxygen. The interaction of sulfide and TiO_2 surface successfully provided the selective organic transformation to sulfoxide, while amines acted as a redox mediator.

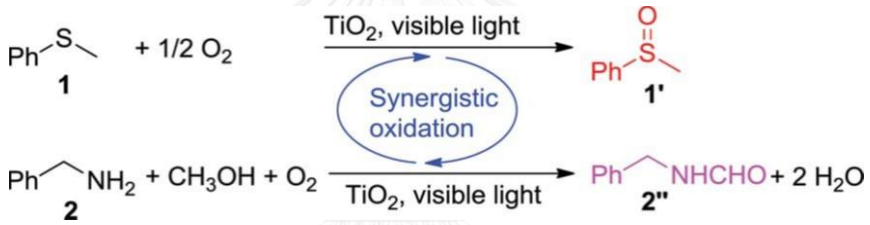

Scheme 2.3 *Synergistic effect between sulfides and amines on the surface of TiO_2 under visible light irradiation [2]*

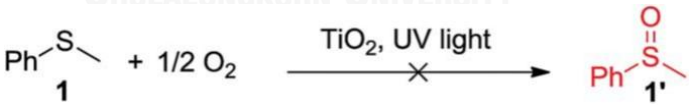

Scheme 2.4 *Aerobic oxidative sulfide on TiO_2 surface under UV irradiation [2]*

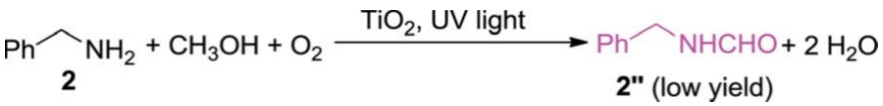

Scheme 2.5 *Aerobic oxidative amine on TiO_2 surface under UV irradiation [2]*

Also, CeO_2/TiO_2 nanotube has recently gained the interest for photocatalytic desulfurization under visible light driven as reported by Lu *et al.* [36] due to the special electron orbital structure and high oxygen storage capability of CeO_2 and the most

well-known TiO_2 photocatalyst forming a composite. As a result, sulfur was removed for more than 90% in the model oil within 5 h. It is noteworthy that TiO_2 composites would attract a great deal of attention to use for organic transformation in oxidation reaction fashion. However, the aforementioned photocatalytic systems still have the tremendous drawbacks from the difficulty in separation of catalyst and product. Therefore, this problem could be solved by incorporating with magnetic materials.

2.5.2 Magnetic metal-ferrite (MFe_2O_4) catalyst for organic transformation

Tiano *et al*. [28] investigated the promising MFe_2O_4 (M= Mg, Fe, Co, Ni, Cu and Zn) as catalytically active ferrite nanoparticles ***(Figure 2.7)*** for photocatalytic degradation of methylene blue (MB) as organic dye pollutants under UV irradiation. It was founded that $MgFe_2O_4$ nanoparticles exhibited the highest photocatalytic activity compared to other transition metal-ferrites as shown in ***Figure 2.8***.

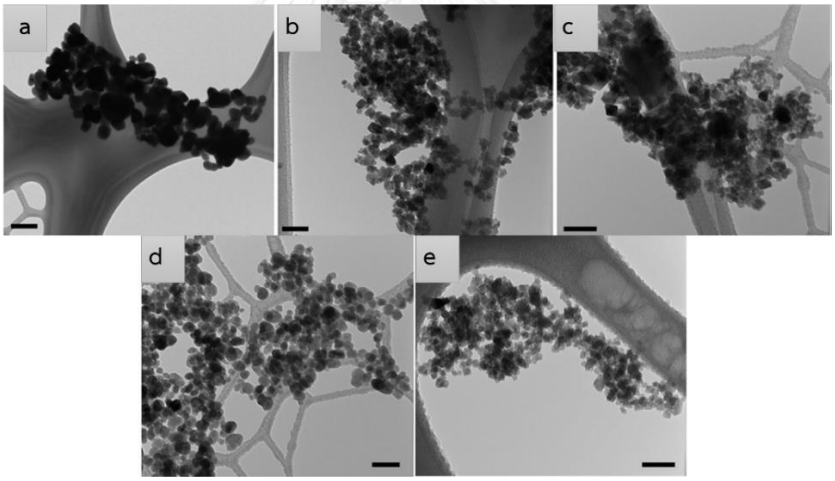

Figure 2.7 *TEM micrographs associated with magnesium (a), cobalt (b), nickel (c), copper (d), and zinc (e) ferrite nanoparticles. All scale bars represent 40 nm [28].*

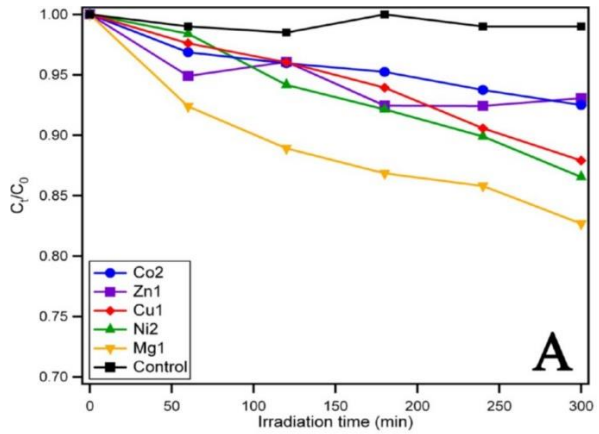

Figure 2.8 *Photodegradation of methylene blue under 366 nm UV irradiation in the presence of magnesium (yellow, ▼), nickel (green, ▲), copper (red, ◆), zinc (purple, ■), and cobalt (blue, ●) ferrite nanoparticles as a function of irradiation time as compared with a control (black, ■) of methylene blue without any nanoparticles present [28].*

Furthermore, Shahid *et al.* [37] also considered $MgFe_2O_4$ as a photocatalyst for the degradation of MB under visible light irradiation with slight difference in the light source from the previous research. The photocatalytic activity of $MgFe_2O_4$ was similar to commercial-TiO_2 (P25) under UV or visible light irradiation.

Interestingly, $MgFe_2O_4$ demonstrated high photostability even after reusing the photocatalyst over ten times under the same condition for photodegradation. Therefore, it is reasonable to assume that $MgFe_2O_4$ is a promising photocatalyst under visible light irradiation.

Additionally, catalytic applications include metal ferrite (MFe_2O_4), where M= Cu, Ni, Co, and Zn are able to conduct in the applications of photocatalytic degradation, reactions of dehydrogenation, oxidation ***(Scheme 2.6)***, alkylation ***(Scheme 2.7)***, C–C coupling, among other processes. Ferrite nanocatalysts can be magnetically recovered from reaction systems and reused up to several runs without significant loss of activity [5].

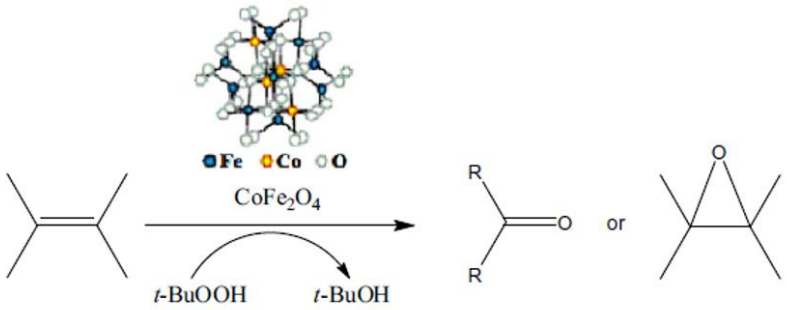

Scheme 2.6 *The oxidation of alkene using $CoFe_2O_4$ catalyst [38]*

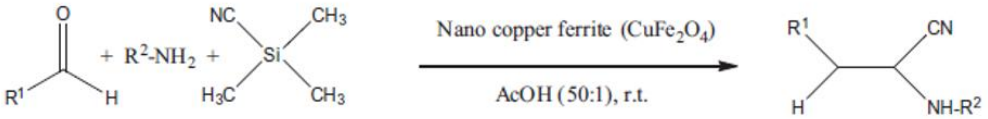

Scheme 2.7 *The synthesis of α-aminonitriles in the presence of nano $CuFe_2O_4$ in water as green solvent at ambient condition [39]*

Moreover, the other metal ferrites have been reported to exhibit catalytic activities and could be useful in organic compound synthesis [40]. Nickel ferrite nanoparticles could catalyze the synthesis of substituted pyrroles under neat conditions reaction at relatively short times (3–4 h) with high yields (70–96%) as shown in ***Scheme 2.8***. The nickel-ferrite catalyst can be easily separated for removing the catalyst by an external magnetic field [41].

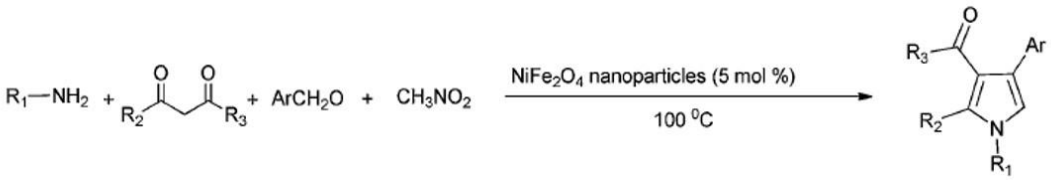

Scheme 2.8 *The preparation of different substituted pyrroles [41]*

According to the previous literature reviews**,** the MFe_2O_4 alone can be active catalysts in various reaction. For this reason, MFe_2O_4 will be the promising candidate for using as catalyst to investigate the efficiency in our focused reaction.

2.5.3 $MgFe_2O_4/TiO_2$ nanocomposites

To develop the function of catalyst, Zhang *et al.* [42] synthesized $MgFe_2O_4/TiO_2$ composite as a photocatalyst. They found that the photodegradation of RhB by single $MgFe_2O_4$ under visible light irradiation was very low. However, when the TiO_2 composited together with $MgFe_2O_4$, the enhanced photocatalytic performance of $MgFe_2O_4/TiO_2$ nanocomposite under UV and visible light irradiation in comparison with single TiO_2 or $MgFe_2O_4$ catalyst was significantly convincing as the promising photocatalyst composite with superparamagnetic properties.

As primarily reviewed, MFe_2O_4 could show the catalytic properties on their own for using in many kinds of organic transformations. Furthermore, $MgFe_2O_4$ nanoparticles have been reported to be the promising candidate to couple with TiO_2 for using under visible light activation; however, they were rarely found in the use for the thiol oxidation. Therefore, we aim at not only investigating the catalytic activity of MFe_2O_4 nanoparticles and $MgFe_2O_4/TiO_2$ nanocomposites to utilize in the aerobic oxidation of thiol reaction which is useful in many research fields as mentioned in previous reports, but also performing the magnetic separation using from MFe_2O_4 nanoparticles for catalyst reusability. Our catalyst system could be an alternative catalyst to be effectively used with dual functions at the same time.

CHAPTER III

EXPERIMENTS

The experimental section is composed of two parts. First part is the synthesis of $MgFe_2O_4$@TiO_2 composites, magnetic ferrite nanoparticles, and the other part is the study of catalytic activity measurements.

The instrument and chemicals which are used for the synthesis of magnetic ferrite nanoparticles and the study of catalytic activity measurements were listed below.

3.1 The instrument

Table 3.1 List of instrument

Characterization techniques	Models
X-ray powder diffraction spectrometer (XRD)	DMAX22002Ultima+ (Rigaku)
Transmission electron microscope (TEM)	JEM-2100 (JEOL)
Fourier Transform Infrared spectrometer (FT-IR)	Impact 410 (Nicolet)
Inductively Coupled Plasma Optical Emission Spectrometer (ICP-OES)	Perkin Elmer Optima 2100
Scanning Electron Microscope-Electron Dispersive X-ray Spectrometer (SEM-EDX)	JSM-5410
Nuclear Magnetic Resonance Spectrometer (NMR)	OXFORD Varian 400 MHz
Centrifuge	Centaur 2 (Sanyo)
Magnetic stirrer	MS 101 (Gem)

3.2 Chemicals

Table 3.2 List of chemicals

Chemicals	Supplier
Iron (III) chloride ($FeCl_3$), AR grade	Aldrich
$MnCl_2.4H_2O$, (99+%)	Aldrich
$CoCl_2.6H_2O$, (99+%)	Aldrich
$CuCl_2$, (99+%)	Aldrich
$NiCl_2$, (99+%)	Aldrich
$ZnCl_2$, (99+%)	Aldrich
$MgCl_2$, (99+%)	Aldrich
Oleic acid ($C_{16}H_{34}O_2$), AR grade	Merck
Sodium hydroxide (NaOH), pellet for analysis	Merck
Ethanol (C_2H_5OH), AR grade	Merck
n-Hexane (C_6H_{14}), AR grade	Lab scan
Acetone, AR grade	Lab scan
1-octadecene ($C_{18}H_{36}$), AR grade	Lab scan
Titanium(IV) butoxide ($Ti(OC_4H_9)_4$), AR grade	Aldrich
Ethylene glycol ($C_2H_6O_2$), AR grade	Aldrich
29% Ammonium hydroxide (NH_4OH), AR grade	Merck
Polyoxyethylene (5) nonylpheylether (Igepal CO-520), reagent grade	Aldrich
2-Propanol, AR grade	Univar
4-Chlorothiophenol (ClC_6H_4SH), AR grade	Aldrich
Methanol-d_4	Aldrich

3.3 Synthesis of magnetic metal ferrite nanoparticles core/ titanium dioxide shell (MFe_2O_4@TiO_2)

The synthesis of titanium dioxide coated MFe_2O_4 (MFe_2O_4@TiO_2) with the average size of 26 nm was tailored by using a reverse-micelle microemulsion process as Figure 3.1

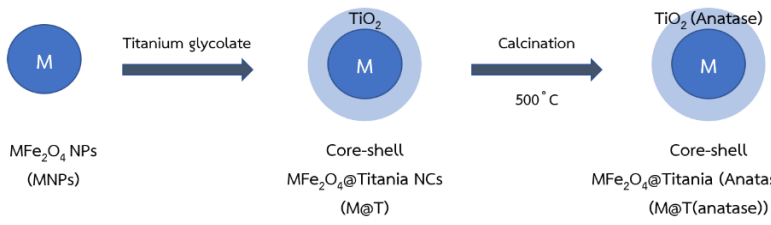

Figure 3.1 *Schematic presentation for the synthesis of magnetic metal ferrite nanocryastals core/ titanium dioxide shell (MFe_2O_4@TiO_2)*

The synthesis of MFe_2O_4@TiO_2 was designed in 3 steps. Firstly, magnetic ferrite NPs (MNPs) was synthesized as the starting materials. Secondly, titanium glycolate was coated onto MNPs using reverse-micelle microemulsion process. Lastly, MFe_2O_4@TiO_2 was calcined at 500 C to tailor the TiO_2 changed to anatase phase.

3.3.1 Synthesis of monodisperse magnetic metal ferrite (MFe_2O_4) NPs

MFe_2O_4 NCs was synthesized using thermal decomposition method which comprised two processes as following in ***Equation 3.1 and 3.2***

$$2FeCl_3 + MCl_2 + 8Na(C_{18}H_{33}O_2) \longrightarrow M^{2+}Fe_2^{3+}(C_{18}H_{33}O_2)^-_8 + 8NaCl \text{---- } \textit{(3.1)}$$

$$MFe_2(C_{18}H_{33}O_2)_8 \xrightarrow{\text{Thermal decomposition}} MFe_2O_4 \text{ NPs} \text{ ---- } \textit{(3.2)}$$

3.3.1.1 Synthesis of metal oleate complexes

The mixed metal ($M^{2+}Fe_2^{3+}$)-oleate complexes or $M^{2+}Fe_2^{3+}(C_{18}H_{33}O_2)_8$, where M^{2+} are Co^{2+}, Ni^{2+}, Mn^{2+}, Fe^{2+} and Cu^{2+} were prepared by reaction of sodium oleate and the metal chlorides (the mixture of Fe^{3+} and M^{2+}= Co^{2+}, Ni^{2+}, Mn^{2+}, Fe^{2+} and Cu^{2+}, respectively [18]. For example, in the synthesis of Co^{2+} $Fe_2^{3+}(C_{18}H_{33}O_2^-)_8$, 4.0 mmol $FeCl_3$, 2.0 mmol $CoCl_2$, 16.0 mmol sodium oleate ($C_{18}H_{33}NaO_2$), 10 mL H_2O, 10 mL ethanol, and 20 mL hexane were mixed and refluxed at 60°C for 4 h. The mixed $Fe_2^{3+}(C_{18}H_{33}O_2^-)_8$ was obtained by the separation of the water phase and subsequent evaporation of the residual ethanol and hexane at 40°C.

3.3.1.2 Synthesis of metal ferrite (MFe_2O_4) NPs

In a typical synthetic procedure for monodisperse mixed metal ferrite nanocrystals, 5.0 g of the mixed metal ($M^{2+}Fe_2^{3+}$)-oleate complex was dissolved in 20 mL 1-octadecene containing 0.40 g oleic acid at room temperature. The temperature program was tuned as the following parameters shown in ***Table 3.3***; the reaction mixture was heated to 320°C with a constant heating rate of 3.3 °C/min [43], and then kept at this temperature for 30 min. When the reaction temperature reached 320 °C, a severe reaction was observed as the initial transparent solution became turbid and brownish black mixture. The resulting solution containing the nanocrystals was then cooled to room temperature and washed with hexane and ethanol. A black precipitate was obtained by centrifugation at 4000 rpm for 5 min.

Finally, the as-synthesized MFe_2O_4 NCs were redispersed in n-hexane and kept in refrigerator.

Table 3.3 Temperature program for the preparation of monodispersed magnetic metal ferrite nanoparticles (MNPs)

Step	Temperature (°C)	Duration (hr.)	Note
1	50	0.15	Vacuum
2	50	1.00	Vacuum
3	320	1.21	At 100 °C flow N_2 gas
4	320	0.30	Flow N_2 gas
5	160	0.05	Flow N_2 gas
6	160	2.00	Flow air
7	40	0.05	Flow air

3.3.2 Synthesis of titanium glycolate precursor

Firstly, ethylene glycol (EG) was added in a 100 mL round bottom flask and then vacuum pumped at 120 C for about 1 hour. After that, the system was cooled down to 30 C and bubbled with nitrogen for about 15 minutes to remove oxygen and water. The solution including titanium butoxide (TBT) was vigorously stirred for 8 hours in the ambient condition. Titanium glycolate was stocked in a vial covered with septum on top and purged with nitrogen gas.

3.3.3 Synthesis of core-shell magnesium ferrite@titanium dioxide nanocomposites (M@T)

The mixture of 84 mL cyclohexane and 9.8 g IGEPAL was magnetically stirred at room temperature. During the continuously stirring, 110 mg magnesium-ferrite NPs had been mixed, the resultant solution would be brownish. Then, 1000 µL titanium glycolate precursor was gradually added into the solution and kept stirring at room temperature overnight. Finally, M@T had been calcined at 500 C for about 2 hours.

3.4 Synthesis of titanium dioxide (TiO_2)

For reactivity-reduced titanium precursor solutions, 0.4 mL of TBT was chelated by mixing with 25 mL of EG under vigorously stirring and continuously bubbled with nitrogen gas for about 10 minutes to remove water and oxygen at room temperature. Then, this system was pierced with nitrogen balloon and kept stirring for a further 24 hours. After that, the above solution was poured into 100 mL of acetone containing with different amount of aqueous solution under magnetically stirring for 1 day aging. The white precipitate was harvested by centrifugation, followed by washing with acetone and ethanol several times to remove residual EG from the surface of titanium glycolate particles. For the heat treatment, the samples were annealed at 500 C for 2 hours with heating rate of 1 C/min.

3.5 Characterization of the as-synthesized MNPs and MFe_2O_4@TiO_2 NCs

The morphology of spherical MNPs and spherical-liked MFe_2O_4@TiO_2 NCs were investigated by using Transmission electron microscope (TEM) a JEOL 2100CX microscope at 200 kV for confirming shapes and sizes. In the preparation of samples, they were done by dropping the sample which was dispersed in hexane on a copper grid and dried at ambient atmosphere.

The crystalline phases of MNPs and MFe_2O_4@TiO_2 NCs were examined by X-ray Diffraction technique (XRD) using Rigaku D/MaX-2200 Ultima-plus instrument with Cu K radiation of 1.5418 A° wavelength at 40kV around 30mA condition. In the preparation of samples, powders samples were packed on a glass holder. The scans of 2-theta were performed in steps of 0.03° over ranging from 20 ° to 80 ° at 25 ℃.

Moreover, the components in term of compositional distributions of each metal which located on MNPs and MFe_2O_4@TiO_2 NCs were investigated by utilizing Scanning electron microscope – Energy dispersive X-ray (SEM-EDX) because of the similar structure of MFe_2O_4 also for being the clear-cut evidence of the compositions of the as-synthesized MFe_2O_4 and MFe_2O_4@TiO_2 NCs.

In addition, the core-shell formation was considered by Fourier transform infrared (FT-IR) spectrometer. The spectra of TiO_2 shell coating on MFe_2O_4 core were determined on an Impact 410 (Nicolet) spectrometer at wavenumber ranging from 400 to 4000 cm^{-1}. Samples were thoroughly mixed with KBr and molded into a pellet form.

Inductively Coupled Plasma-Optical Emission Spectrometry (ICP-OES) was used for determining the quantity of various metal atoms, which are related to the quantity of as-synthesized MNPs and MNPs in the composite. For the sample preparations, all metal components were digested with aqua regia, which was blended from HNO_3 and HCl in the volume ratio of 1:3, and then the solution was filtered with 0.45 μm pore size filter. The solution was eventually analyzed the quantity of metal components by ICP-OES.

3.6 Catalytic activity measurement

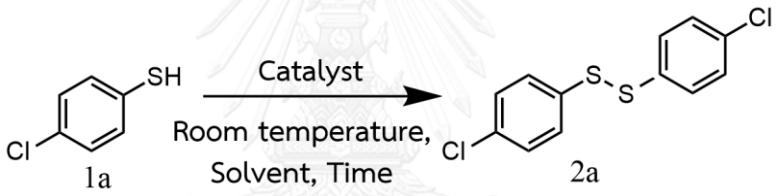

The catalytic activity was measured after 50 mg of 4-chlorothiophenol **(1a)** was dissolved in 3.50 mL solvent together with the various amounts of catalysts and kept stirring at ambient temperature in the dark and light conditions at various times. Then, the catalyst will be separated out of the solution using an external magnet. The solution was evaporated and subsequently dissolved with methanol-d_4 for nuclear magnetic resonance (NMR) measurement.

3.7 Calculation of catalytic efficiency

In order to calculate the percent of conversion ***(Equation 3.3)***, nuclear magnetic resonance (NMR) was utilized; the ratio of areas of the signals from 1,2-Bis(4-chlorophenyl) disulfane **(2a)**, ^{1}H NMR (CD_3OD, 400 MHz): δ 7.50 (d, *J* = 8.5 Hz, 4H), 7.37 (d, J = 8.6 Hz, 4H) and the signals from ^{1}H NMR (CD_3OD, 400 MHz): δ 7.25 (dd, *J* = 19.4, 8.5 Hz, 6H) of **(1a)** were used to identify the efficiency of each catalyst.

$$\%conversion = \frac{Integration\ of\ product}{Integration\ of\ starting + Integration\ of\ product} \qquad (3.3)$$

CHAPTER IV

RESULTS AND DISCUSSIONS

Herein, this part substantially focuses in the discussions from experimental results. To begin with the first part, metal-ferrite nanoparticles (MNPs) and the MNPs@TiO_2 composites were characterized for the structures, compositions, sizes, and shapes. Secondly, catalytic efficiency of MNPs was investigated under various conditions. Finally, the catalytic reusability was investigated for indicating their stability and potential as efficient catalysts.

4.1 Characterization of the as-synthesized metal-ferrite (MFe_2O_4) nanoparticles

Monodisperse MFe_2O_4 nanoparticles were synthesized by thermal decomposition of $M^{2+}Fe_2^{3+}$-oleate complexes dissolved in 1-octadecene at 320°C under N_2 ambient.

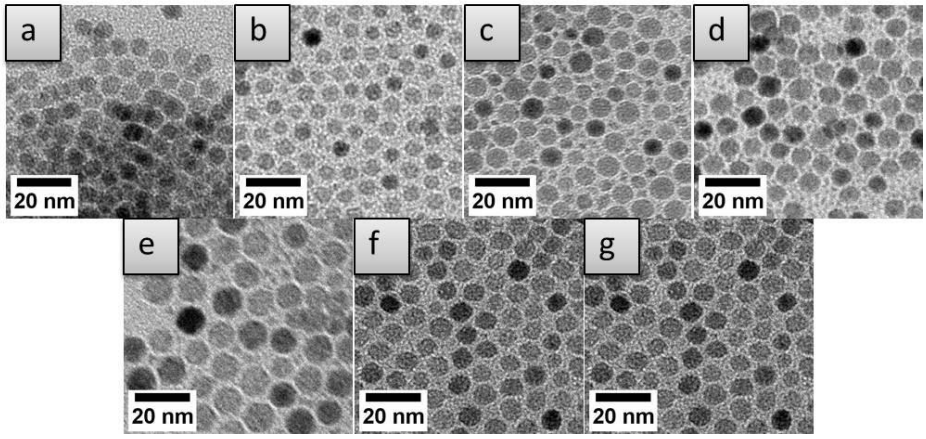

Figure 4.1 *TEM micrographs of metal ferrite magnetic nanoparticles of different compositions: (a) manganese (Mn)-, (b) nickel (Ni)-, (c) cobalt (Co)-, (d) iron (Fe)-, (e) copper (Cu)-, (f) magnesium (Mg)-, and (g) zinc (Zn) ferrites, respectively.*

The sizes and shapes of as-synthesized MFe_2O_4 nanoparticles were characterized using transmission electron microscopy (TEM). ***Figure 4.1*** shows the TEM micrographs of different metal-ferrite nanoparticles. The average diameters of the spheres were in the range of 6-13 nm ($MnFe_2O_4$ 6.73 nm, $NiFe_2O_4$ 6.11 nm, $CoFe_2O_4$ 12.00 nm, Fe_3O_4 13.30 nm, $CuFe_2O_4$ 11.85 nm, $MgFe_2O_4$ 9.57 nm, and

$ZnFe_2O_4$ 13.37 nm) as shown in ***Figure 4.1***. Particularly, metal-ferrite nanoparticles, with the sizes below 20 nm, would display superparamagnetic behavior that they were strongly attracted to an external magnet. In contrast, paramagnetic behavior would be observed when an external magnetic field was removed as every single metal-ferrite (MFe_2O_4) nanoparticles are separately dispersed in hexane. The crystalline and structure of MFe_2O_4 nanoparticles were also confirmed by using diffractions technique (XRD). As shown in ***Figure 4.2***, the peak positions and relative intensity of all diffraction peaks of corresponding metal-ferrite nanoparticles matched well with each of JCPDS standard.

The representative XRD spectra matched well with the corresponding MFe_2O_4 in JCPDS standard; however, board peaks and low intensity of XRD spectra from each MFe_2O_4 nanoparticles were common characteristics appeared found in nanoparticles samples. Because all XRD patterns cannot be clearly identified the type of metal ferrite because of their very similar XRD pattern, whether the metal ferrite phases obtained were pure or there were major impurities from the magnetite (Fe_3O_4) and maghemite (γ-Fe_2O_3) phases was further studied. Scanning Electron Microcopy coupled with Energy Dispersive X-ray (SEM-EDX) was used for elemental analysis. Atomic percentage of each element in various ferrite structures were analyzed as shown in ***Figure 4.3*** to confirm the presence of different metal ferrite structures with low impurities from the two iron oxide phases.

According to the percentage of each component from the EDX data, molar ratios in some types of MFe_2O_4 structure followed the empirical formula such as $CuFe_2O_4$ and Fe_3O_4 (Magnetite). However, some MFe_2O_4 did not follow the empirical formula such as $CoFe_2O_4$, where the ratio between Co and Fe is equal (1:1). This observation was likely due to the similar size of Co and Fe, so it was possible that Fe might be replaced with Co into the structure. On the contrary, the overloading of Fe in the structure of $MgFe_2O_4$, $ZnFe_2O_4$, $MnFe_2O_4$, and $NiFe_2O_4$ was observed, and it might be implied that proposed metal-ferrite structures may mix with other ferrimagnetic phases of Fe_3O_4 and γ-Fe_2O_3 resulting in the M:Fe ratio of 1:2 was not observed in these ferrite structures as shown in ***Figure 4.3***. Apart from the elemental analysis,

SEM-EDX showed an elemental mapping of MFe_2O_4 nanoparticles and the distribution of metal in ferrite structures. For example, elemental mapping of $CuFe_2O_4$ nanoparticles is shown in ***Figure 4.4***. These mapping indicated a possibility of $CuFe_2O_4$ structure as Cu ***(Figure 4.4b)*** was well distributed and coexist with Fe ***(Figure 4.4C)***.

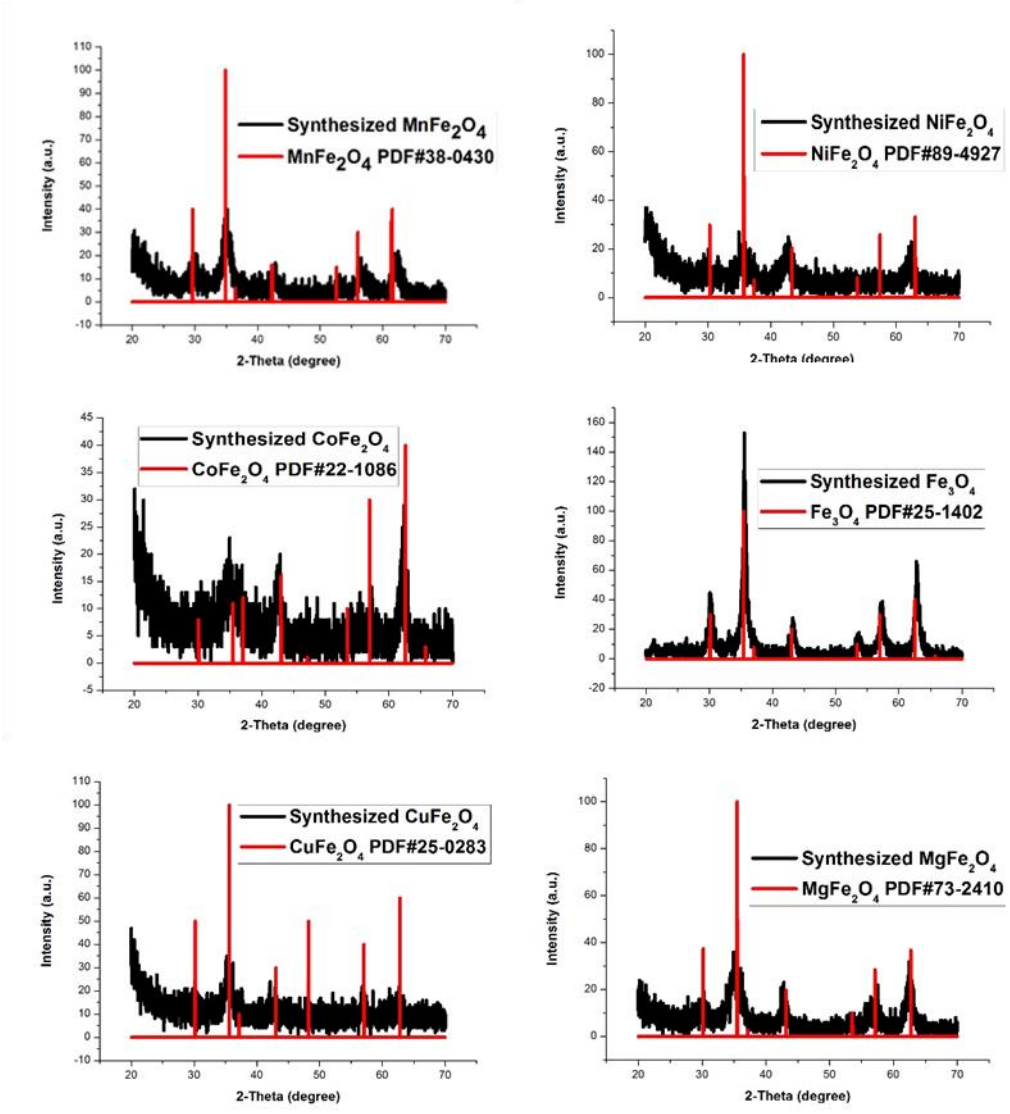

Figure 4.2 *XRD patterns of synthesized crystalline metal ferrite magnetic nanoparticles (MFe_2O_4) of (a) manganese (Mn), (b) nickel (Ni), (c) cobalt (Co), (d) iron (Fe), (e) copper (Cu), (f) magnesium (Mg), and (g) zinc (Zn) ferrites, respectively compared with the references of standard patterns.*

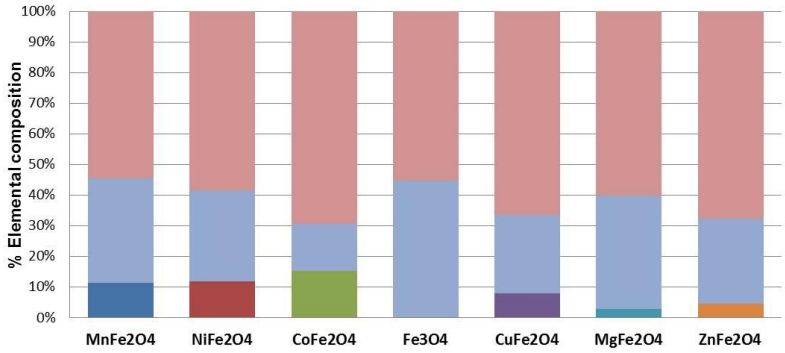

Figure 4.3 *Atomic percent of composed elements: Mn, Ni, Co, Cu, Mg, Zn, Fe, and O indicated by dark blue, deep red, light green, purple, indigo, orange, light blue, and light red, respectively, in metal ferrite structures* MFe_2O_4 *using SEM-EDX elemental analysis.*

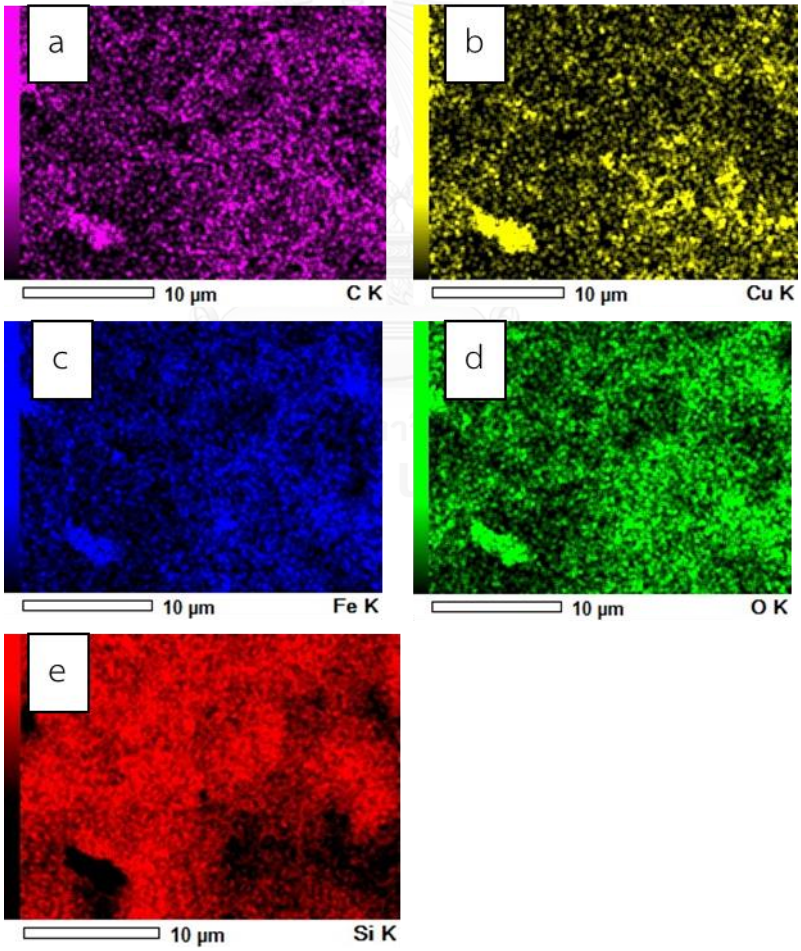

Figure 4.4 *The mapping of* $CuFe_2O_4$ *using SEM-EDX elemental analysis with signal from* ***(a)*** *C,* ***(b)*** *Cu,* ***(c)*** *Fe,* ***(d)*** *O, and* ***(e)*** *Si.*

4.2 Characterization of titanium dioxide (TiO_2)

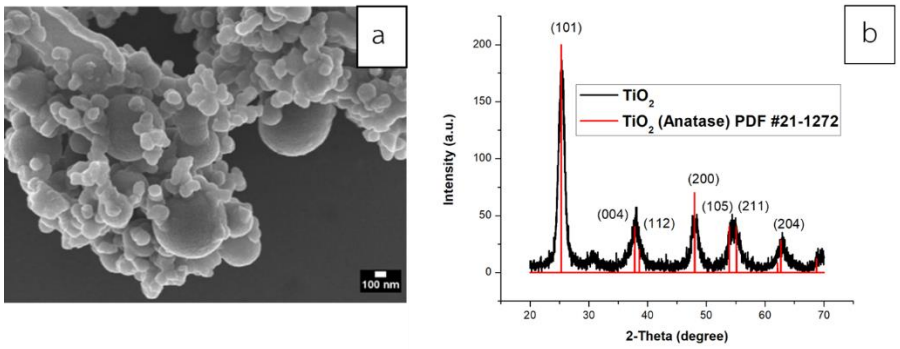

Figure 4.5 (a) *SEM of the titanium dioxide (TiO_2), and* ***(b)*** *XRD pattern of the TiO_2 reference PDF#21-1272*

In order to compare the efficiency of the catalytic composite, pure TiO_2 particles were prepared as a reference material of high catalytic activity. The TiO_2 nanoparticles was characterized by using SEM as shown in ***Figure 4.5a***. TiO_2 was agglomerated after calcination to transform the phase of titanium dioxide to be anatase ***(Figure 4.5b)***, which is the active phase for using as photocatalyst because of the slow rate of charge recombination [44]. For this phenomenon, the excited electron would stay in the excited state for photo-redox reaction and available for oxidation reaction for longer than the other two phases, which are rutile and brookite [44].

4.3 Characterization of $MgFe_2O_4$@TiO_2 nanocomposites

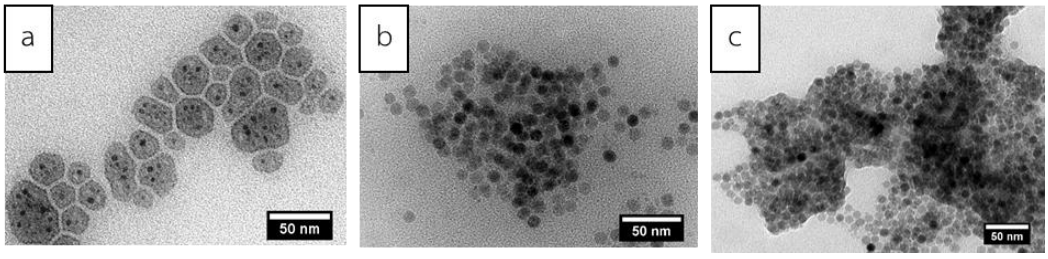

Figure 4.6 *TEM micrographs of the as-synthesized $MgFe_2O_4$ @ TiO_2* ***(a)*** *core-shell,* ***(b)*** *incomplete core-shell nanocomposites before calcination, and* ***(c)*** *the $MgFe_2O_4$ @ TiO_2 after calcined at 500 C*

Core-shell structure of $MgFe_2O_4$@TiO_2 nanocomposites were confirmed by Fourier- Transform Infrared spectrometer (FT-IR) and SEM-EDX. According to ***Figure 4.6a*** *and* ***b,*** there were the core-shell imperfection of some parts of magnesium-ferrite nanoparticles after synthesized. Conversely, after the as-synthesized $MgFe_2O_4$@TiO_2 nanocomposites were calcined at 400 C, the nanocomposites would agglomerate together; however, some of them still were partially covered with titanium dioxide as shown in ***Figure 4.6c***. The FT-IR bands at 2800-2900 cm^{-1}, which were the position of C-H stretching from oleic acid from $MgFe_2O_4$, as labeled on the FT-IR spectra in ***Figure 4.7a*** of $MgFe_2O_4$ @ TiO_2 were significantly decreased comparing with original $MgFe_2O_4$ in ***Figure 4.7b***. The reasons for this observation can be either that TiO_2 was coated onto $MgFe_2O_4$ and replaced the original coating or that the organic compound (oleic acid) has been combusted after calcination, or both.

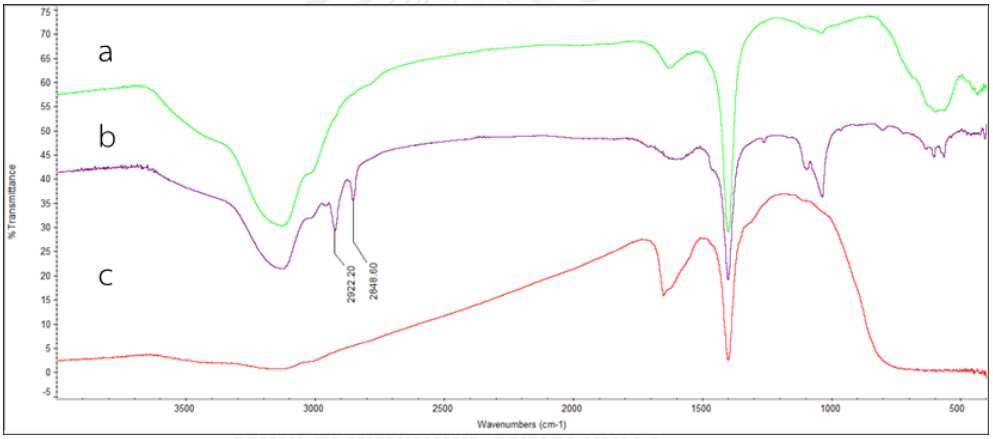

Figure 4.7 *FT-IR spectra of* ***(a)*** *$MgFe_2O_4$@TiO_2 nanocomposites,* ***(b)*** *$MgFe_2O_4$ nanoparticles, and* ***(c)*** *TiO_2 nanoparticles.*

To investigate the core-shell structure, ***Figure 4.8*** shows that the XRD spectrum of as-synthesized $MgFe_2O_4$@TiO_2 nanocomposites did not matched well with JCPDS standards of neither anatase nor rutile. We assumed that the tiny quantity of TiO_2 may be in amorphous form on the surface of magnetic nanoparticles after calcination. Therefore, the XRD pattern mainly showed the structure of $MgFe_2O_4$@TiO_2 as the structure of $MgFe_2O_4$ as shown in ***Figure 4.8***.

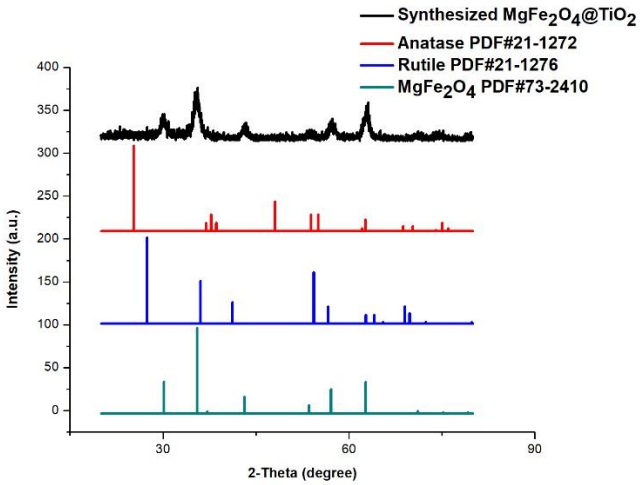

Figure 4.8 *XRD patterns of synthesized crystalline $MgFe_2O_4$@TiO_2 nanocomposites compared with the references of standard patterns.*

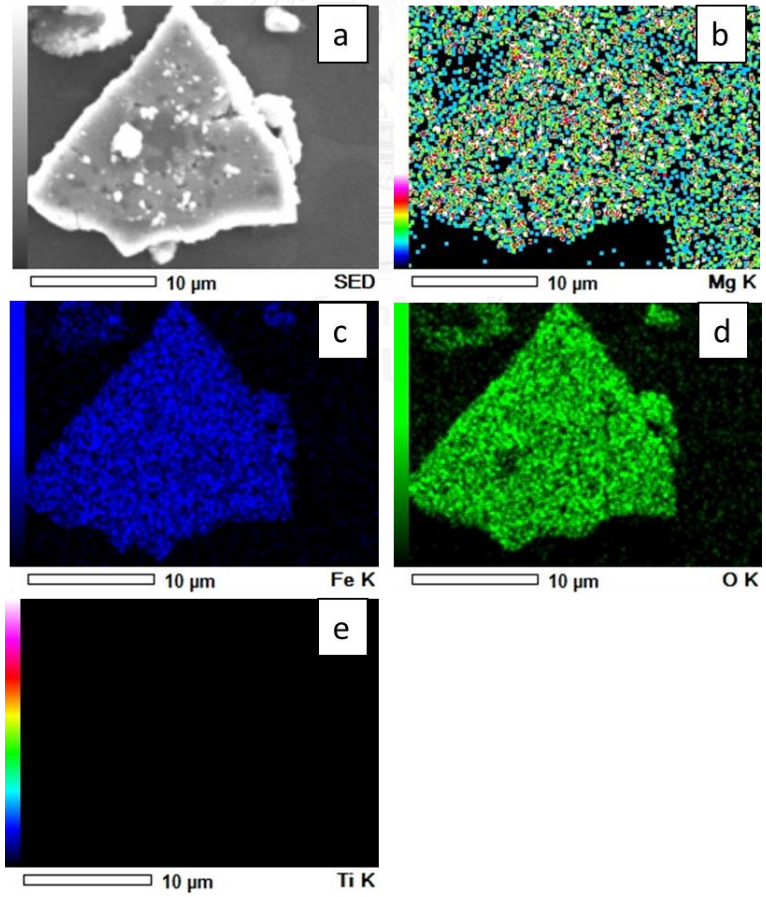

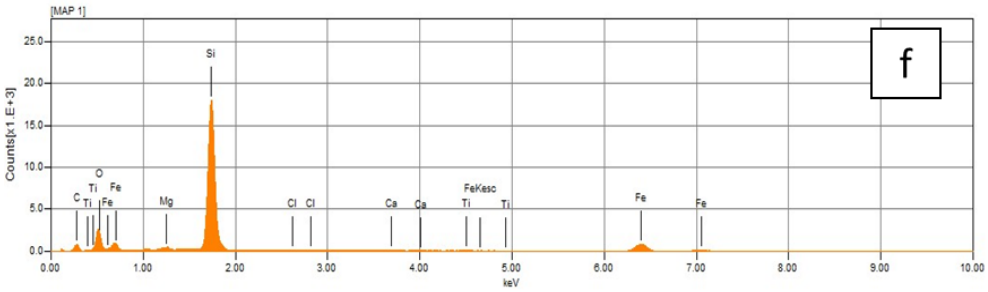

Figure 4.9 *The mapping of $MgFe_2O_4$@TiO_2 core-shell structure using SEM-EDX elemental analysis* ***(a)*** *original SEM image, and elemental maps of* ***(b)*** *Mg,* ***(c)*** *Fe,* ***(d)*** *O,* ***(e)*** *Ti, and* ***(f)*** *the elemental composition ratio graph*

Furthermore, ***Figure 4.9a-d*** shows that the elemental compositions in $MgFe_2O_4$@TiO_2 core-shell structure was mainly covered with 0.67% Mg, 8.11% Fe, and 21.24% O from the core-shell structure mapping; however, Ti signal was not shown up in the mapping micrograph ***(Figure 4.9e)***. However, ***Figure 4.9f*** showed that the signal of titanium was detected; hence, we claim that titanium was the one of elemental composition, yet it was in small amount (0.1% Ti) in the as-synthesized $MgFe_2O_4$@TiO_2 nanocomposites. From this result, we are able to assume that the core-shell structure was not entirely harvested.

4.3 Catalytic activity of $MgFe_2O_4$@TiO_2 nanocomposites in the transformation of 4-chlorothiophenol

Table 4.1 Effect of types of catalysts

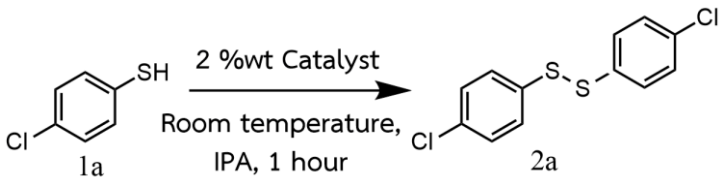

Entries	Catalyst	%conversion[a]	
		Dark condition	Light condition
1	TiO_2	100	100
2	$MgFe_2O_4$	100	100
3	$MgFe_2O_4$@TiO_2	100	100

[a] Reaction conditions: 4-chlorothiophenol (50.0 mg), catalysts (2% wt), 2-propanol (3.6 mL) stirred within 1 hour under room temperature. Percentage of conversion value was calculated by NMR.

In the part of catalytic activity of each catalyst of interest, the oxidation reaction of 4-chlorothiophenol was completely catalyzed by all types of catalysts studied. Previously, we expected that the final product would harvest after photocatalytic process under visible light irradiation on the $MgFe_2O_4$ composites. Unfortunately, $MgFe_2O_4$@TiO_2 nanocomposites are also active under dark condition with high efficiency as shown in ***Table 4.1***. Although $MgFe_2O_4$@TiO_2 nanocomposites were the excellent catalyst, $MgFe_2O_4$ was also surprisingly active as complete conversion was obtained as shown in ***Entry 2***. As a result, TiO_2 is not essentially required to design on catalyst for harvesting the complete conversion. The single $MgFe_2O_4$ nanoparticles have outstanding properties to be the catalyst for the aerobic oxidation of thiol as well. For this reason, we would explore the effect of each metal in ferrite structures for determining the different capacities under dark condition in the upcoming part.

4.4 Catalytic activity in the transformation of 4-chlorothiophenol with various metal-ferrite (MFe_2O_4) nanoparticles

In order to compare the catalytic activity of metal-ferrites, the concentration of materials need to be determined and control. However, molar concentration of nanoparticles cannot be calculated from an empirical formula. Every nanoparticle consists of several units of empirical formula (n(MFe_2O_4)). Accordingly, we need to specifically calculate the number of used nanoparticles by using the information following the ***Equation 4.1-4.2.***

The molar concentration of magnetic metal ferrite nanoparticles (MNPs) in ***Table 4.2*** can be calculated by ***Equation 4.1-4.2.***

$$\boldsymbol{n = \frac{V}{v}} \qquad \textit{(4.1)}$$

Where;

n *= time from number of formula units per particles*

V *= volume of metal ferrite empirical formulae*

v *= volume of metal ferrite nanoparticles calculated from particle size obtained by TEM*

$$mol\ of\ nanoparticles = \frac{g}{M \times n} \qquad \textit{(4.2)}$$

Where;

g *= grams of metal ferrite nanoparticles*

M *= empirical formula weight of metal ferrite*

n *= time from number of formula units per particles* ***(Equation 4.1)***

Table 4.2 Determination of the concentration of MFe_2O_4 nanoparticles for using as catalyst

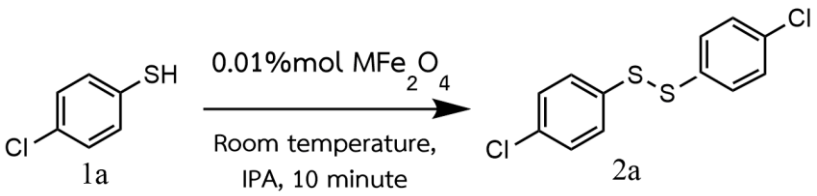

Entries	Catalyst	Size (nm)	n	Concentration by atoms (molar)	Concentration by particles (molar)
1	$ZnFe_2O_4$	12.64	1057	9.87×10^{-6}	6.17×10^{-11}
2	Fe_3O_4	13.30	16019	9.87×10^{-6}	7.83×10^{-10}
3	$MnFe_2O_4$	6.73	2238	9.87×10^{-6}	1.43×10^{-9}
4	$CuFe_2O_4$	11	6900	9.87×10^{-6}	1.41×10^{-9}
5	$NiFe_2O_4$	6.11	1647	9.87×10^{-6}	4.49×10^{-9}
6	$MgFe_2O_4$	11.98	12609	9.87×10^{-6}	5.89×10^{-9}
7	$CoFe_2O_4$	10.28	7168	9.87×10^{-6}	9.09×10^{-9}

To determine the efficiency of metal ferrite catalysts at the 0.1 %mol catalysts loading, the catalytic efficiency of each catalysts cannot be differentiated as all types of catalysts showed the highest percent of conversion in the oxidation of 4-chlorothiophenol in ***Table 4.3***. For this reason, the loading of catalyst amount was reduced to explore the most remarkable metal ferrite in catalytic efficiency as shown in ***Table 4.4.***

4.4.1 Catalytic oxidation of 4-chlorothiophenol in 2-propanol

Table 4.3 Effect of metals in ferrite structure

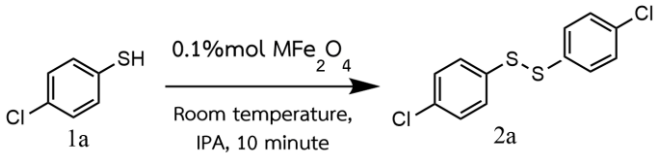

Entries	Catalyst	Conversion[a] (%)
1	$ZnFe_2O_4$	100
2	Fe_3O_4	100
3	$MnFe_2O_4$	100
4	$CuFe_2O_4$	100
5	$NiFe_2O_4$	100
6	$MgFe_2O_4$	100
7	$CoFe_2O_4$	100

[a] Reaction conditions: 4-chlorothiophenol (50.0 mg), MFe_2O_4 (0.1% mol), 2-propanol (3.6 mL) stirred within 10 min under room temperature. Percentage of conversion value was calculated by ^{1}H-NMR.

Table 4.4 Effect of time at 0.01 mol% loading metal ferrite catalysts

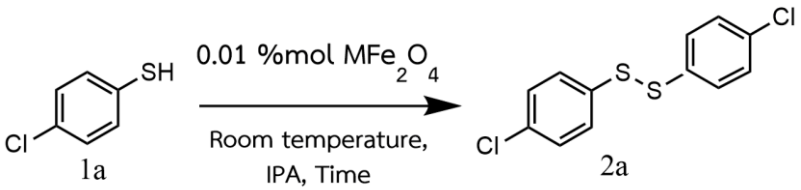

Entries	Catalyst	Time (min)	Conversion (%)
1	$ZnFe_2O_4$	10	100
2	$ZnFe_2O_4$	60	100
3	Fe_3O_4	10	29
4	Fe_3O_4	60	93
5	$MnFe_2O_4$	10	95
6	$MnFe_2O_4$	60	94
7	$CuFe_2O_4$	10	100
8	$CuFe_2O_4$	60	100
9	$NiFe_2O_4$	10	60
10	$NiFe_2O_4$	60	72
11	$MgFe_2O_4$	10	71
12	$MgFe_2O_4$	60	78
13	$CoFe_2O_4$	10	81
14	$CoFe_2O_4$	60	88

[a] Reaction conditions: 4-chlorothiophenol (50.0 mg), MFe_2O_4 (0.01% mol), iso-propanol (3.6 mL) stirred within reaction time under room temperature. Percentage of conversion value was calculated by NMR.

From the catalytic data in ***Table 4.4***, $ZnFe_2O_4$ and $CuFe_2O_4$ notably performed catalytic conversions highly to 100% in comparison with original ferrite structure as Fe_3O_4 and other metal ferrite catalysts. It was a crystal-clear evidence that the metal in ferrite structures significantly performed high catalytic activity [45]. Moreover, metals also prominently improved the catalytic rate while comparing reaction time between 10 min to 60 min on each of metal ferrite structure. Interestingly, the ferrites with three highest catalytic activity were Cu, Zn, and Mn respectively, all of which were in the

group with the half (Mn) and full (Cu and Zn) electron occupancy in d-orbital. If can be predicted that electron localized in these metal ferrite structures would be more stable than other ferrite structures that have the available d-orbital allowing to the sites that can retard the catalytic oxidation of 4-chlorothiophenol. For better utilizing as efficient green catalysts, the remarkable $CuFe_2O_4$ and $ZnFe_2O_4$ catalysts would be studied in the catalytic oxidation in water as discussed in ***Section 4.4.2.***

4.4.2 Catalytic oxidation of 4-chlorothiophenol in water using $CuFe_2O_4$ and $ZnFe_2O_4$

Catalytic oxidation of 4-chlorothiophenol with between $CuFe_2O_4$ and $ZnFe_2O_4$ nanoparticles in water were investigated and the results are shown in ***Table 4.5 and 4.6***

Table 4.5 Effect of reaction time in the reaction of 4-chlorothiophenol using $ZnFe_2O_4$ catalyst in water

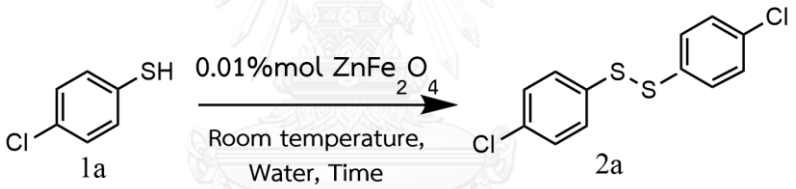

Entries	Time	Conversion (%)
1	1 h	31
2	1 day	42
3	2 day	100

Basically, $ZnFe_2O_4$ worked very well together with $CuFe_2O_4$ but in water $ZnFe_2O_4$ exhibited lower catalytic activity. Nonetheless, $ZnFe_2O_4$ still slowly catalyzed in the oxidation reaction up to 42 % within 24 h as shown in ***Entry 1-2*** *in* ***Table 4.5***. Eventually, the starting substance would gradually convert to product after 2 days to obtain the high percent of conversion which depended on reaction time. Thus, it was reasonable to assume that the more time consumed, the more reaction catalyzed.

Table 4.6 Effect of reaction time in the reaction of 4-chlorothiophenol using $CuFe_2O_4$ catalyst in water

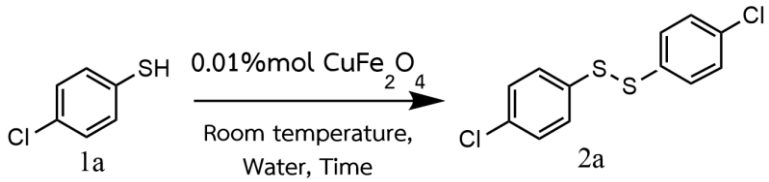

Entries	Time	Conversion (%)
1	1 h	37
2	1 day	80
3	2 day	98

According to ***Table 4.6***, the oxidation was activated by $CuFe_2O_4$ as catalyst would dramatically increase the rate of catalysis from 1 h to 24 h. Then, the catalysis of oxidation was almost completed within 2 days. Even if ***Table 4.4*** demonstrated that $CuFe_2O_4$ successfully overcame the oxidation reaction within 10 minutes, but in that condition 2-propanol was used as a solvent, and the starting materials can adequately dissolve into the reaction mixture. For reaction using water as a solvent, 4-chlorothiophenol was slightly dissolved in the solution; thus, the chemical reaction would reasonably take more time to complete. According to ***Table 4.5*** and ***Table 4.6***, $CuFe_2O_4$ and $ZnFe_2O_4$ catalyst could be the promising catalysts for converting to the final product within the same reaction time. With magnetic property of metal ferrite catalysts, we aim to observe the number of cycles for reusability to differentiate the efficiency as reusable catalysts between this couple of catalyst candidates in the ***Section 4.5***.

4.5 Reusability of $ZnFe_2O_4$ and $CuFe_2O_4$ nanoparticles

4.5.1 Reusability of $ZnFe_2O_4$ catalyst

In practical the $ZnFe_2O_4$ nanoparticles were reused in the amount of 0.01 % mol $ZnFe_2O_4$ nanoparticles for the oxidation of **1a** to **2a** as shown in ***Table 4.5***. To determine the number of reused cycles, the reactions were established under similar conditions in water. When the reaction was completed, the $ZnFe_2O_4$ nanoparticles were magnetically recovered without further purification. A new 4-chlorothiophenol with fresh water was added in the original vial under the same condition. As in ***Figure 4.10***, $ZnFe_2O_4$ nanoparticles could be used for two times without any change in activity. Then, the catalytic activity was decreased to about 68% conversion at the third run of reaction. If it is possibly predicted, the limitation of oxidation state of Zn form has been only Zn^{2+} in ferrite structure so it cannot be reduced or oxidized to any other forms. For this reason, the reusable would mainly come from the reduction or oxidization of Fe species in ferrite structure as shown in ***Figure 4.11a***. Zn leaching was also studied by ICP-OES after finishing each run of the reaction and very small amount (~ 0.1%) of Zn was leached. For this reason, the amount of Zn in the final product can be negligible; therefore, $ZnFe_2O_4$ can be used without the metal contamination in water.

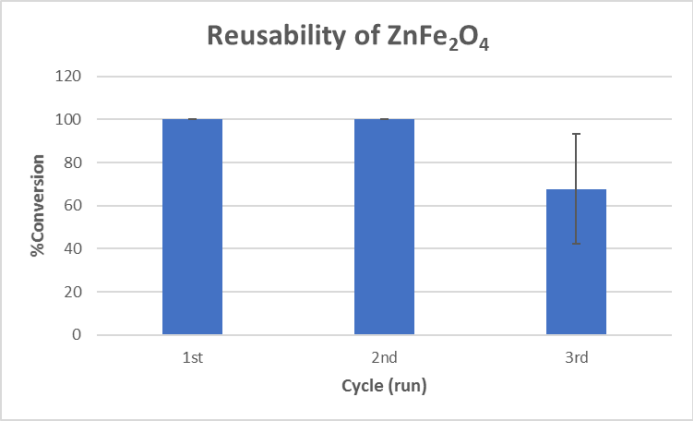

Figure 4.10 *Percent conversion of reused $ZnFe_2O_4$ catalyst in the presence of 0.01% mol catalyst within 2 days*

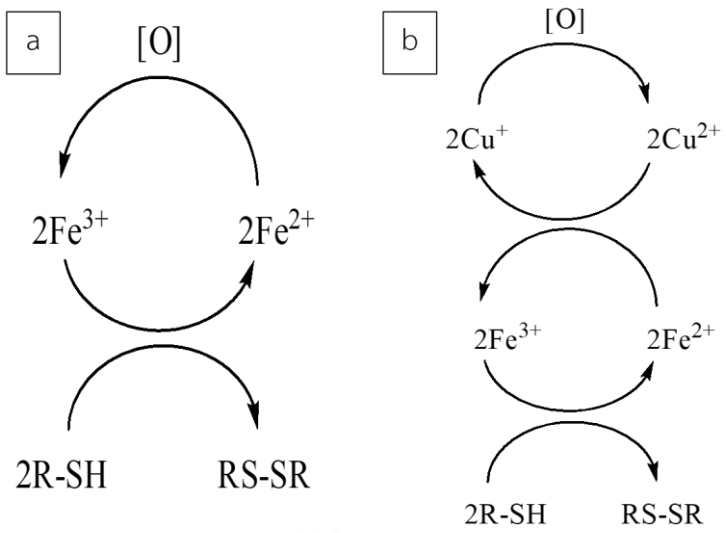

Figure 4.11 *Proposed catalytic mechanism of* ***(a)*** *$ZnFe_2O_4$ and* ***(b)*** *$CuFe_2O_4$.*

4.5.2 Reusability of $CuFe_2O_4$ catalyst

The reusability of 0.01 % mol $CuFe_2O_4$ catalyst was tested in the oxidation of **1a** to **2a** as shown in ***Table 4.6***. All experimental settings were performed as similar to ***Section 4.5.1.***

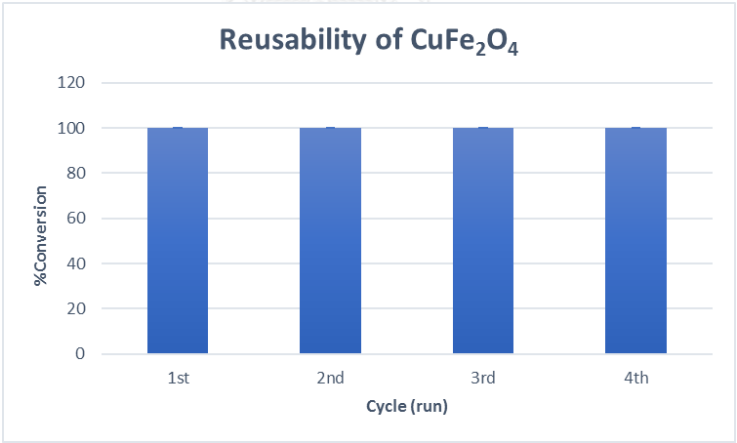

Figure 4.12 *Percent conversion of reused $CuFe_2O_4$ catalyst in the presence of 0.01% mol catalyst within 2 days*

After the fourth cycle, the percent conversion within 2 day using $CuFe_2O_4$ was still satisfactory ***(Figure 4.12)***; however, beyond the fourth runs, magnetic response was significantly dropped down, but the catalytic activity was still effective, most likely due to the absorption of organic products covering over catalytic surface [46] as well as the phase transformation of the crystal structure as shown in ***Figure 4.14***. For these

reasons, the magnetic response was decreased despite the remaining $CuFe_2O_4$ structure but with some parts transformed to α-Fe_2O_3 (Hematite) which does not exhibit the magnetic response as it is antiferromagnetic. For the catalytic activity, after the 4th cycle, the percent of conversion steadily stay at 100%, so it might be the cause of the remained $CuFe_2O_4$ and α-Fe_2O_3 which can effectively catalyze by the effect of Fe in the hematite structure as shown in ***Figure 4.11b***. The derivative of 4-chlorothiophenol would obtained after the couple between $RS^{\cdot}$ and $RS^{\cdot}$ which was generated from R-SH reacting with reactive oxygen ($O_2^{\cdot -}$) as proposed in ***Figure 4.13***.

$$2O_2 + 2e^- \longrightarrow 2O_2^{\cdot -}$$
$$2Cu^+ \longrightarrow 2Cu^{2+} + 2e^-$$
$$2Fe^{3+} + 2e^- \longrightarrow 2Fe^{2+}$$
$$R\text{-}SH + O_2^{\cdot -} \longrightarrow R\text{-}S^{\cdot} + OOH^-$$
$$R\text{-}S^{\cdot} + R\text{-}S^{\cdot} \longrightarrow RS\text{-}SR$$

Figure 4.13 *Proposed mechanism of $CuFe_2O_4$ in the aerobic oxidation of thiol compound*

Furthermore, we have evaluated the amount of Cu in the final product of the oxidation reaction, there was only tiny amount (~0.002%) of Cu that was detected by ICP-OES.

For better reusability, the surface of catalyst should be modified with high porous material not only to protect the magnetic properties from the phase transformation, but also increase the surface area for higher catalytic area on nanoparticles. Hence, it would be preferable to use $CuFe_2O_4$ nanoparticles for it is an effective catalyst with low cost and an easy handling.

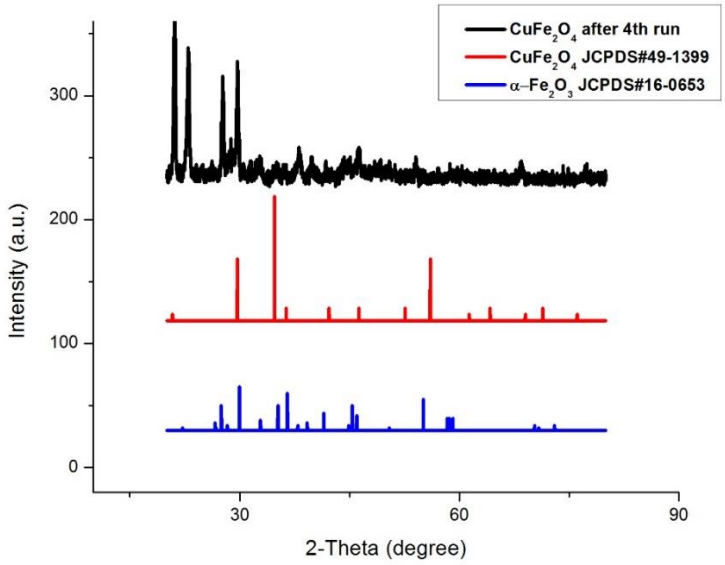

Figure 4.14 *XRD pattern of $CuFe_2O_4$ catalyst after 4th cycle of reuse upon the oxidation of 4-chlorothiophenol*

CHAPTER V

CONCLUSON

Successfully, the thermal decomposition by using iron oleate as starting materials, oleic acid as surfactant, and 1-octadecene as solvent was used to synthesize uniformed MFe_2O_4 nanoparticles with various metals including Mg, Fe, Co, Ni, Cu, and Mn in spherical shape with the diameter of 6-13 nm. $MgFe_2O_4$ nanoparticles were conducted with much afford to modify their surface with TiO_2 for using as multifunctional photocatalyst. Nonetheless, $MgFe_2O_4/TiO_2$ nanocomposites were not completely formed core-shell structure yet $MgFe_2O_4$ and TiO_2 nanoparticles were able to catalyze even without light irradiation. For this observation, they lead to the interesting property considering the valuable ability of each single MFe_2O_4 nanoparticles for utilizing in the novel function as magnetic catalysts in oxidative 4-chlorothiophenol reaction.

Every MFe_2O_4 nanoparticle potentially demonstrate complete conversion original of thiol compound to the oxidative form of 4-chlorothiophenol been in 2-propanol as solvent. After investigation, Green Chemistry of this catalytic reaction has been alternative way to explore this reaction in water which is environmental friendly solvent. $CuFe_2O_4$ nanoparticles was dominantly catalyzed the oxidation reaction of 4-chlorothiophenol up to 100% conversion in aqueous solution under dark condition. Moreover, $CuFe_2O_4$ can be magnetically recovered from reaction systems and reused up to the forth runs without any significantly loss of catalytic activity, which was more profitable and more environmental benign for using as magnetic catalytic materials.

In summary, this work demonstrated a novel magnetic MFe_2O_4 nanocatalysts that were effectively utilized in the selected oxidative organic transformation. Also, the magnetic MFe_2O_4 nanoparticles in this work were interesting to be used in the aspect of green chemistry for solving environmental problems by using the simple magnetic materials. Eventually, it needs further improvement to potentially reuse for obtaining

high yield which will lead to widely uses in other organic transformations and is likely to conduct through versatile applications in the future.

REFERENCES

[1] Lang, X., Hao, W., Leow, W.R., Li, S., Zhao, J., and Chen, X. Tertiary amine mediated aerobic oxidation of sulfides into sulfoxides by visible-light photoredox catalysis on TiO2. Chemical Science 6(8) (2015): 5000-5005.

[2] Lang, X., Leow, W.R., Zhao, J., and Chen, X. Synergistic photocatalytic aerobic oxidation of sulfides and amines on TiO2 under visible-light irradiation. Chemical Science 6(2) (2015): 1075-1082.

[3] Lu, X., Li, X., Qian, J., Miao, N., Yao, C., and Chen, Z. Synthesis and characterization of CeO2/TiO2 nanotube arrays and enhanced photocatalytic oxidative desulfurization performance. Journal of Alloys and Compounds 661 (2016): 363-371.

[4] Daghrir, R., Drogui, P., and Robert, D. Modified TiO2 For Environmental Photocatalytic Applications: A Review. Industrial & Engineering Chemistry Research 52(10) (2013): 3581-3599.

[5] Kharisov, B.I., Dias, H.V.R., and Kharissova, O.V. Mini-review: Ferrite nanoparticles in the catalysis. Arabian Journal of Chemistry (2014).

[6] Pang, Y.L., Lim, S., Ong, H.C., and Chong, W.T. Research progress on iron oxide-based magnetic materials: Synthesis techniques and photocatalytic applications. Ceramics International 42(1, Part A) (2016): 9-34.

[7] Akbarzadeh, A., Samiei, M., and Davaran, S. Magnetic nanoparticles: preparation, physical properties, and applications in biomedicine. Nanoscale Research Letters 7(1) (2012): 144.

[8] Tang, B., Wang, G., Zhuo, L., Ge, J., and Cui, L. Facile Route to α-FeOOH and α-Fe2O3 Nanorods and Magnetic Property of α-Fe2O3 Nanorods. Inorganic Chemistry 45(13) (2006): 5196-5200.

[9] Zhang, D., Du, X., Shi, L., and Gao, R. Shape-controlled synthesis and catalytic application of ceria nanomaterials. Dalton Transactions 41(48) (2012): 14455-14475.

[10] Zaera, F. Nanostructured materials for applications in heterogeneous catalysis. Chemical Society Reviews 42(7) (2013): 2746-2762.

[11] Wu, W., Changzhong, J., and Roy, V.A.L. Recent progress in magnetic iron oxide-semiconductor composite nanomaterials as promising photocatalysts. Nanoscale 7(1) (2015): 38-58.

[12] Sanchez, C., Belleville, P., Popall, M., and Nicole, L. Applications of advanced hybrid organic-inorganic nanomaterials: from laboratory to market. Chemical Society Reviews 40(2) (2011): 696-753.

[13] Jariwala, D., Sangwan, V.K., Lauhon, L.J., Marks, T.J., and Hersam, M.C. Carbon nanomaterials for electronics, optoelectronics, photovoltaics, and sensing. Chemical Society Reviews 42(7) (2013): 2824-2860.

[14] Bartelmess, J., Quinn, S.J., and Giordani, S. Carbon nanomaterials: multi-functional agents for biomedical fluorescence and Raman imaging. Chemical Society Reviews 44(14) (2015): 4672-4698.

[15] Witt, D. Recent Developments in Disulfide Bond Formation. Synthesis 2008(16) (2008): 2491-2509.

[16] Rajabi, F., Naserian, S., Primo, A., and Luque, R. Efficient and Highly Selective Aqueous Oxidation of Sulfides to Sulfoxides at Room Temperature Catalysed by Supported Iron Oxide Nanoparticles on SBA-15. Advanced Synthesis & Catalysis 353(11-12) (2011): 2060-2066.

[17] Mandal, B. and Basu, B. Recent advances in S-S bond formation. RSC Advances 4(27) (2014): 13854-13881.

[18] Sun, S., et al. Monodisperse MFe2O4 (M = Fe, Co, Mn) Nanoparticles. Journal of the American Chemical Society 126(1) (2004): 273-279.

[19] Wang, J., Chen, Q., Hou, B., and Peng, Z. Synthesis and Magnetic Properties of Single-Crystals of MnFe2O4 Nanorods. European Journal of Inorganic Chemistry 2004(6) (2004): 1165-1168.

[20] Deng, H., Chen, H., and Li, H. Synthesis of crystal MFe2O4 (M = Mg, Cu, Ni) microspheres. Materials Chemistry and Physics 101(2–3) (2007): 509-513.

[21] Pradhan, P., et al. Comparative evaluation of heating ability and biocompatibility of different ferrite-based magnetic fluids for hyperthermia application. J Biomed Mater Res B Appl Biomater 81(1) (2007): 12-22.

[22] Mazario, E., Herrasti, P., Morales, M.P., and Menendez, N. Synthesis and characterization of CoFe2O4 ferrite nanoparticles obtained by an electrochemical method. Nanotechnology 23(35) (2012): 355708.

[23] Mathew, D.S. and Juang, R.-S. An overview of the structure and magnetism of spinel ferrite nanoparticles and their synthesis in microemulsions. Chemical Engineering Journal 129(1–3) (2007): 51-65.

[24] Ammar, S., et al. Magnetic properties of ultrafine cobalt ferrite particles synthesized by hydrolysis in a polyol medium. Journal of Materials Chemistry 11(1) (2001): 186-192.

[25] Park, J., et al. Ultra-large-scale syntheses of monodisperse nanocrystals. Nat Mater 3(12) (2004): 891-895.

[26] Bao, N., Shen, L., Wang, Y., Padhan, P., and Gupta, A. A Facile Thermolysis Route to Monodisperse Ferrite Nanocrystals. Journal of the American Chemical Society 129(41) (2007): 12374-12375.

[27] Colmenares, J.C. and Luque, R. Heterogeneous photocatalytic nanomaterials: prospects and challenges in selective transformations of biomass-derived compounds. Chemical Society Reviews 43(3) (2014): 765-778.

[28] Tiano, A.L., et al. Correlating Size and Composition-Dependent Effects with Magnetic, Mössbauer, and Pair Distribution Function Measurements in a Family of Catalytically Active Ferrite Nanoparticles. Chemistry of Materials 27(10) (2015): 3572-3592.

[29] Ge, W. and Wei, Y. Iodine-catalyzed oxidative system for 3-sulfenylation of indoles with disulfides using DMSO as oxidant under ambient conditions in dimethyl carbonate. Green Chemistry 14(7) (2012): 2066-2070.

[30] Zottola, M.A., Beigel, K., Soni, S.-D., and Lawrence, R. Disulfides as Cyanide Antidotes: Evidence for a New In Vivo Oxidative Pathway for Cyanide Detoxification. Chemical Research in Toxicology 22(12) (2009): 1948-1953.

[31] Maddanimath, T., Khollam, Y.B., Aslam, M., Mulla, I.S., and Vijayamohanan, K. Self-assembled monolayers of diphenyl disulphide: a novel cathode material for rechargeable lithium batteries. Journal of Power Sources 124(1) (2003): 133-142.

[32] Craig, D., Davidson, W.L., and Juve, A.E. Tetramethylthiuram disulfide vulcanization of extracted rubber. V. Low molecular products and the mechanism of zinc oxide activation. Journal of Polymer Science 6(2) (1951): 177-187.

[33] Shah, D.P. Pesticidal composition comprising sulphur, a fungicide and an agrochemical excipient. 2012, Google Patents.

[34] Nakata, K. and Fujishima, A. TiO2 photocatalysis: Design and applications. Journal of Photochemistry and Photobiology C: Photochemistry Reviews 13(3) (2012): 169-189.

[35] Lang, X., Hao, W., Leow, W.R., Li, S., Zhao, J., and Chen, X. Tertiary amine mediated aerobic oxidation of sulfides into sulfoxides by visible-light photoredox catalysis on TiO2. Chem. Sci. 6(8) (2015): 5000-5005.

[36] Lu, X., Li, X., Qian, J., Miao, N., Yao, C., and Chen, Z. Synthesis and characterization of CeO 2 /TiO 2 nanotube arrays and enhanced photocatalytic oxidative desulfurization performance. Journal of Alloys and Compounds 661 (2016): 363-371.

[37] Shahid, M., et al. Photocatalytic degradation of methylene blue on magnetically separable MgFe2O4 under visible light irradiation. Materials Chemistry and Physics 139(2–3) (2013): 566-571.

[38] Kooti, M. and Afshari, M. Magnetic cobalt ferrite nanoparticles as an efficient catalyst for oxidation of alkenes. Scientia Iranica 19(6) (2012): 1991-1995.

[39] Gharib, A., Noroozi Pesyan, N., Vojdani Fard, L., and Roshani, M. Catalytic Synthesis ofα-Aminonitriles Using Nano Copper FerriteCuFe2O4under Green Conditions. Organic Chemistry International 2014 (2014): 1-8.

[40] Ceylan, S., Friese, C., Lammel, C., Mazac, K., and Kirschning, A. Inductive Heating for Organic Synthesis by Using Functionalized Magnetic Nanoparticles

Inside Microreactors. Angewandte Chemie International Edition 47(46) (2008): 8950-8953.

[41] Moghaddam, F.M., Koushki Foroushani, B., and Rezvani, H.R. Nickel ferrite nanoparticles: an efficient and reusable nanocatalyst for a neat, one-pot and four-component synthesis of pyrroles. RSC Adv. 5(23) (2015): 18092-18096.

[42] Zhang, L., He, Y., Wu, Y., and Wu, T. Photocatalytic degradation of RhB over MgFe2O4/TiO2 composite materials. Materials Science and Engineering: B 176(18) (2011): 1497-1504.

[43] Park, J., et al. Ultra-large-scale syntheses of monodisperse nanocrystals. Nat Mater 3(12) (2004): 891-5.

[44] Dahl, M., Liu, Y., and Yin, Y. Composite Titanium Dioxide Nanomaterials. Chemical Reviews 114(19) (2014): 9853-9889.

[45] Hudson, R., Feng, Y., Varma, R.S., and Moores, A. Bare magnetic nanoparticles: sustainable synthesis and applications in catalytic organic transformations. Green Chem. 16(10) (2014): 4493-4505.

[46] Vindedahl, A.M., Strehlau, J.H., Arnold, W.A., and Penn, R.L. Organic matter and iron oxide nanoparticles: aggregation, interactions, and reactivity. Environ. Sci.: Nano 3(3) (2016): 494-505.

APPENDIX

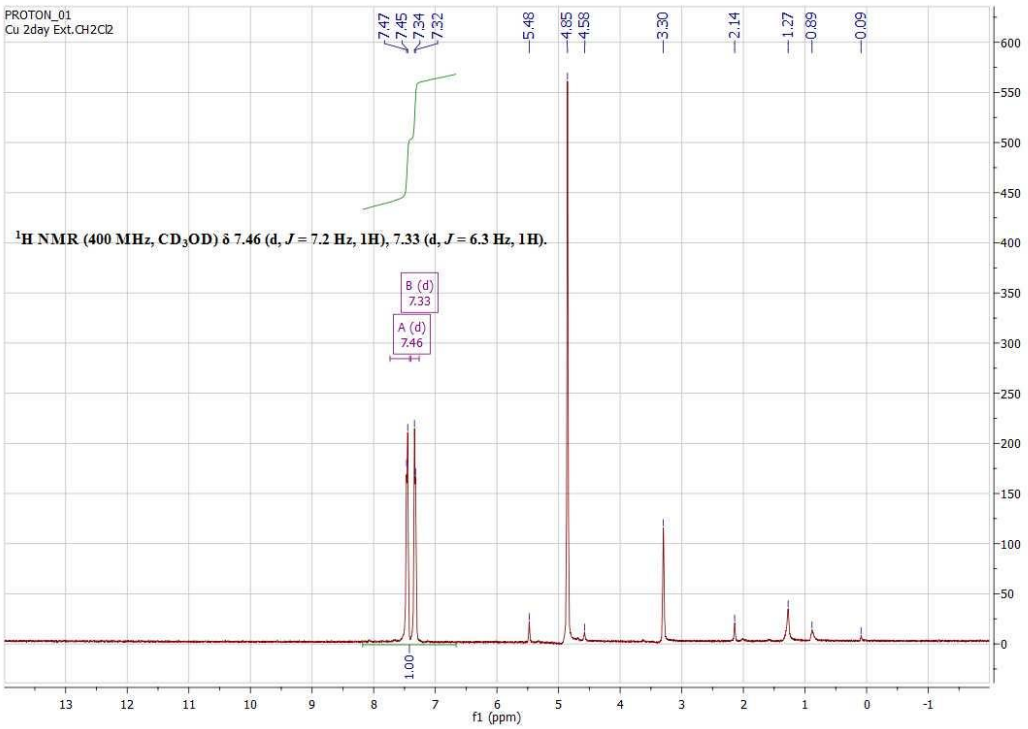

Figure A1 *NMR spectra of complete oxidative conversion from (1a) to (2a)*

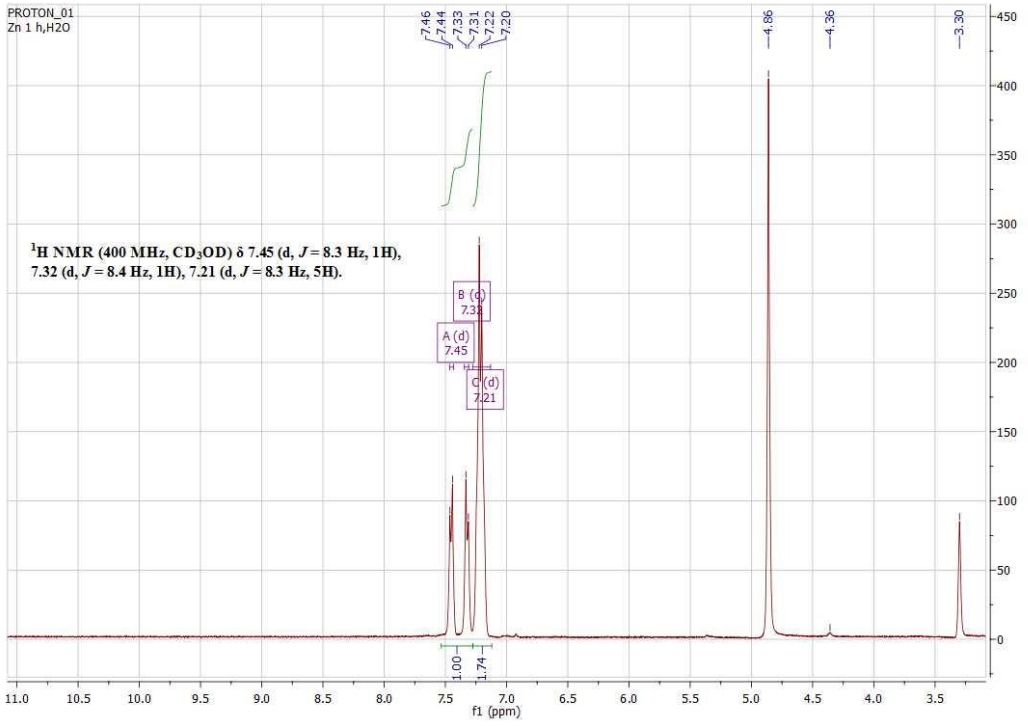

Figure A2 *NMR spectra of incomplete oxidative conversion from (1a) to (2a)*

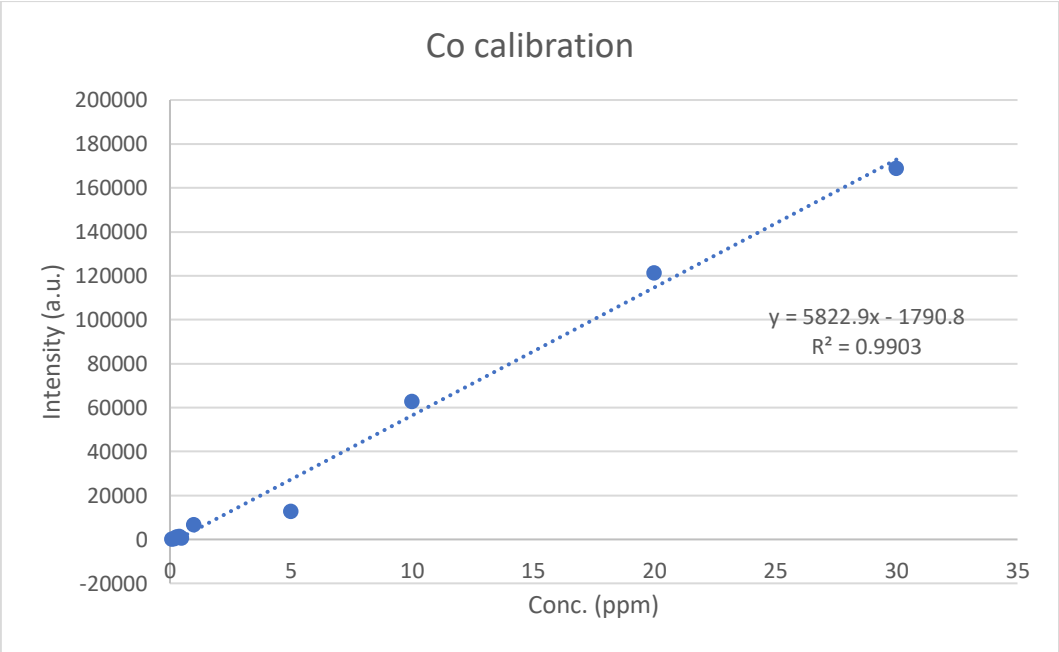

Figure A3 *Calibration curve of $CoFe_2O_4$ for calculating concentration by ICP-OES*

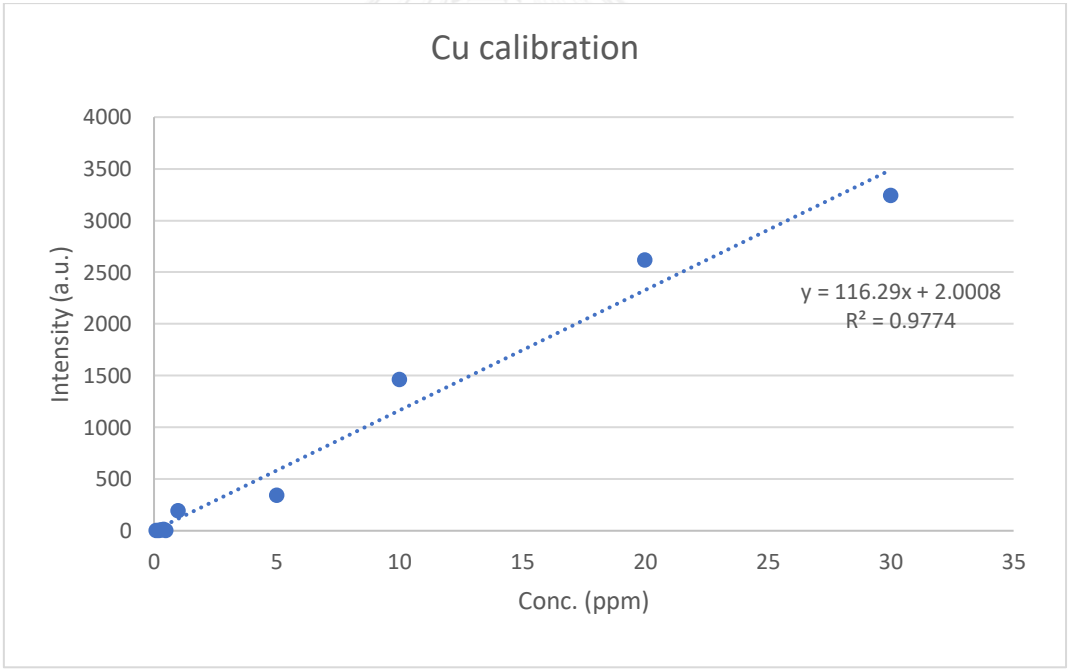

Figure A4 *Calibration curve of $CuFe_2O_4$ for calculating concentration by ICP-OES*

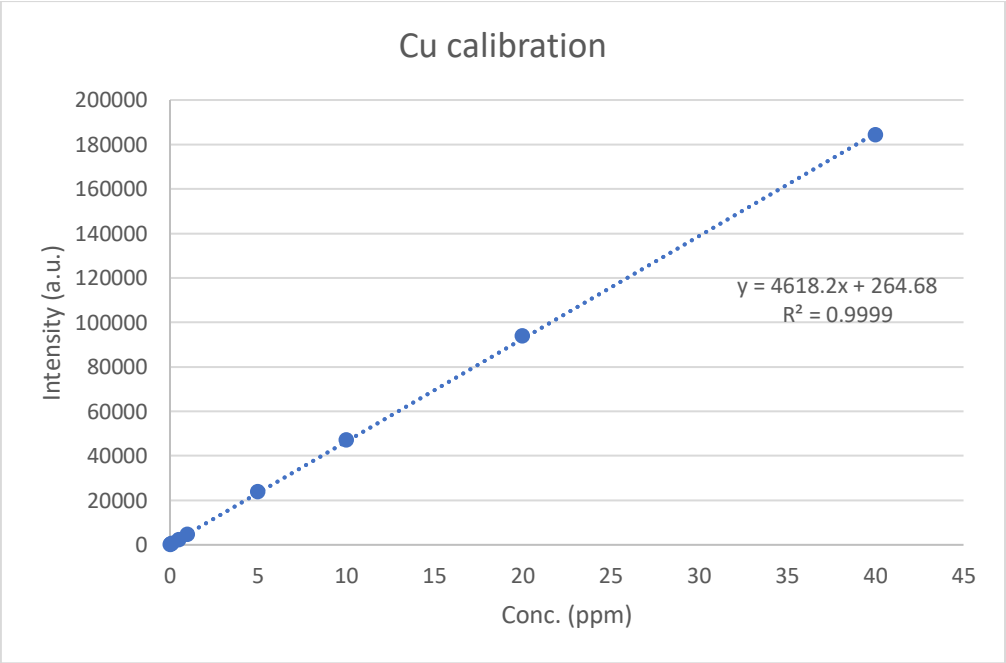

Figure A5 *Calibration curve of $CuFe_2O_4$ for calculating metal leaching by ICP-OES*

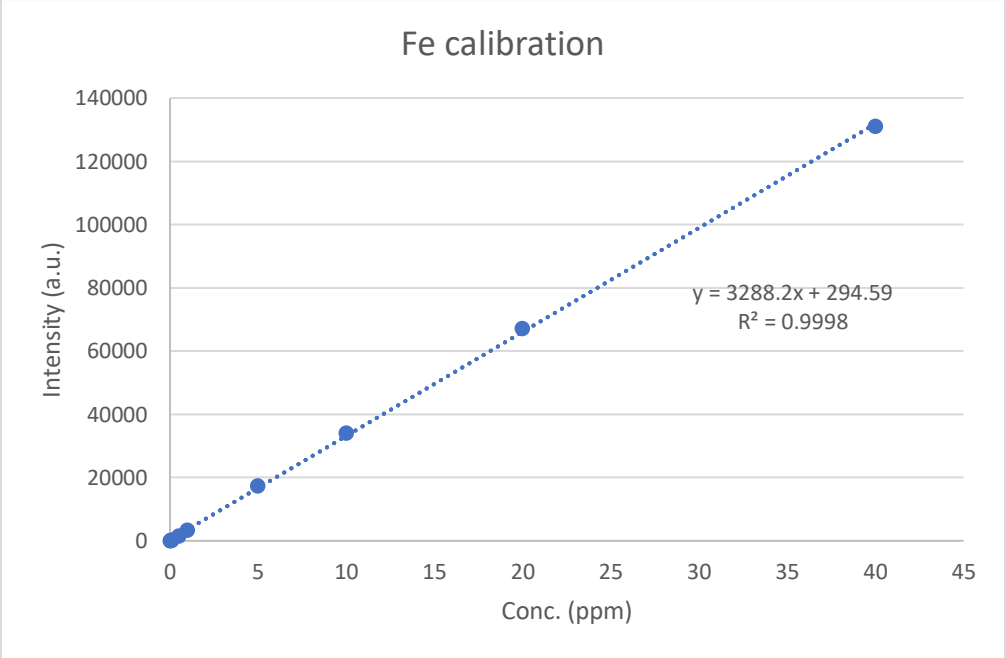

Figure A6 *Calibration curve of Fe_3O_4 for calculating metal leaching by ICP-OES*

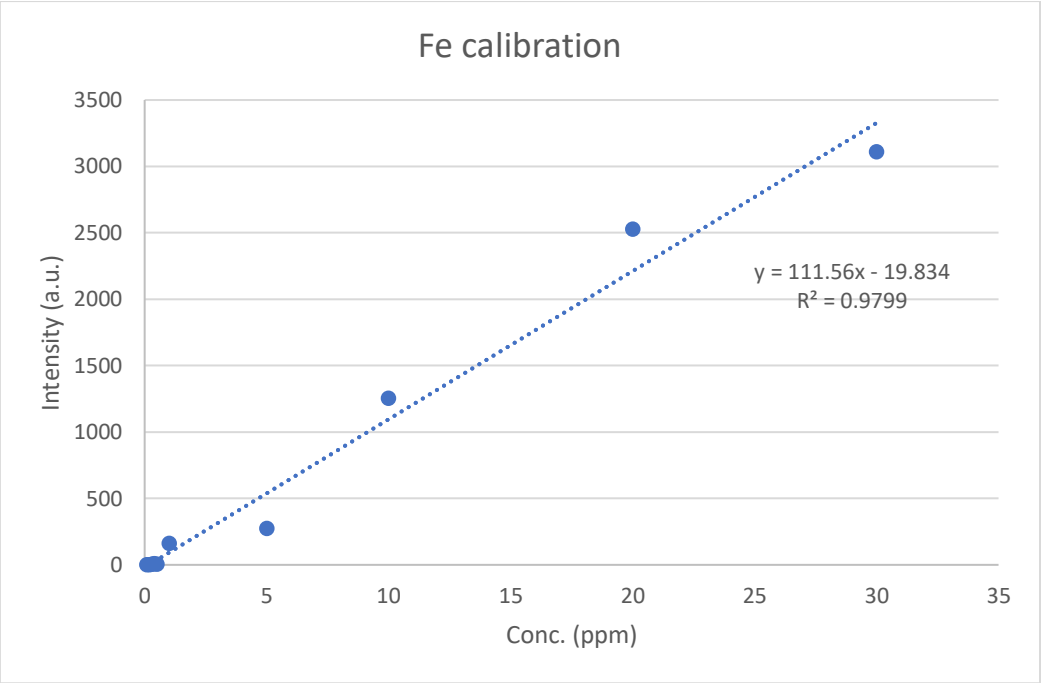

Figure A7 *Calibration curve of Fe_3O_4 for calculating concentration by ICP-OES*

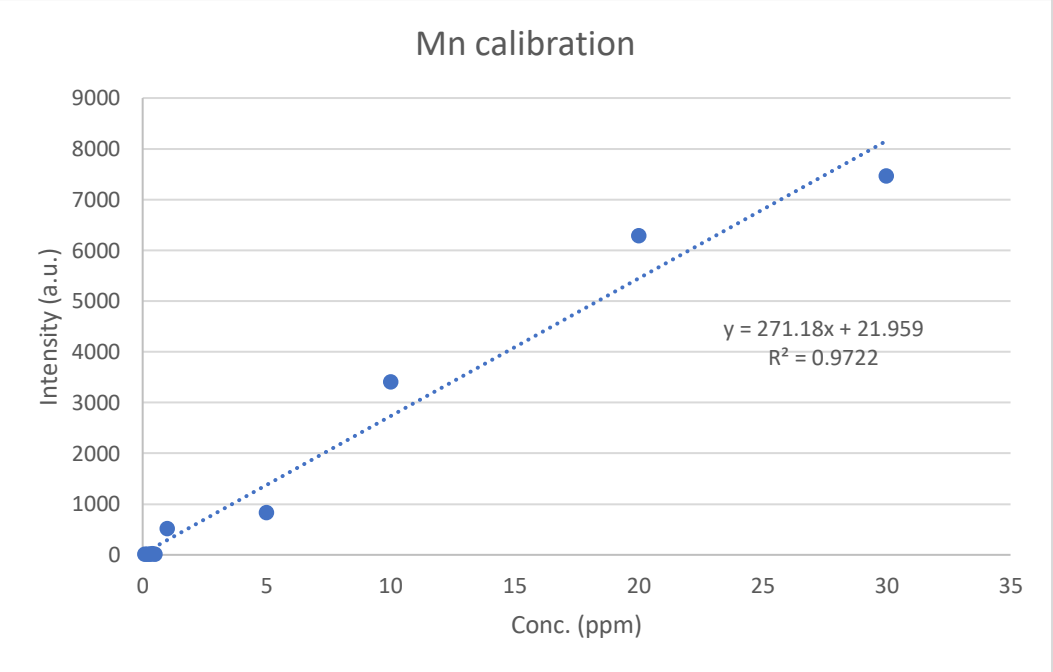

Figure A8 *Calibration curve of $MnFe_2O_4$ for calculating concentration by ICP-OES*

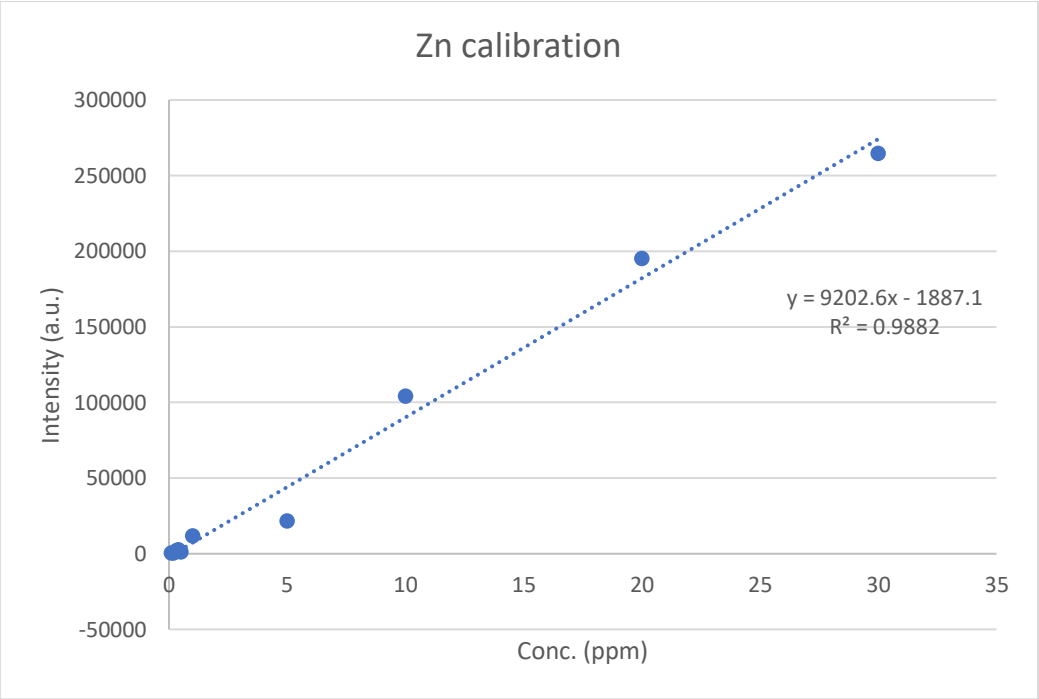

Figure A9 *Calibration curve of $ZnFe_2O_4$ for calculating concentration by ICP-OES*

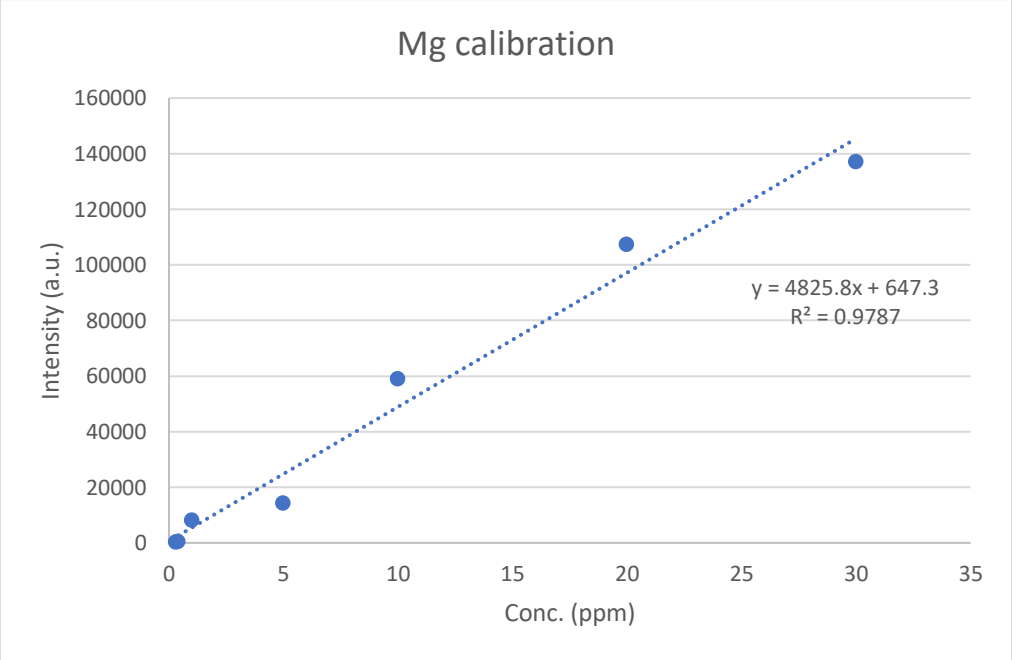

Figure A10 *Calibration curve of $MgFe_2O_4$ for calculating concentration by ICP-OES*

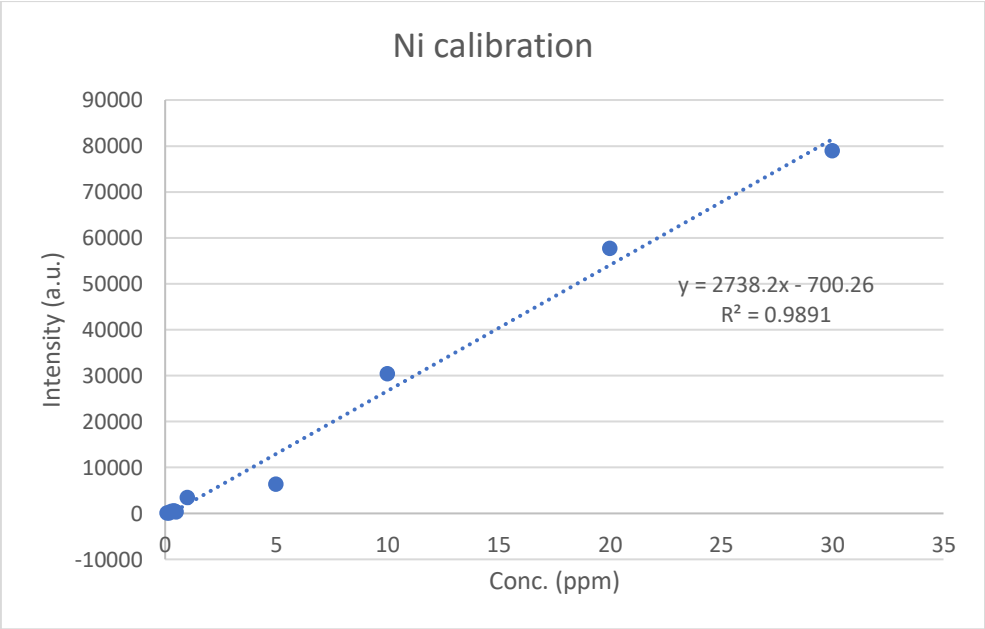

Figure A11 *Calibration curve of $NiFe_2O_4$ for calculating concentration by ICP-OES*

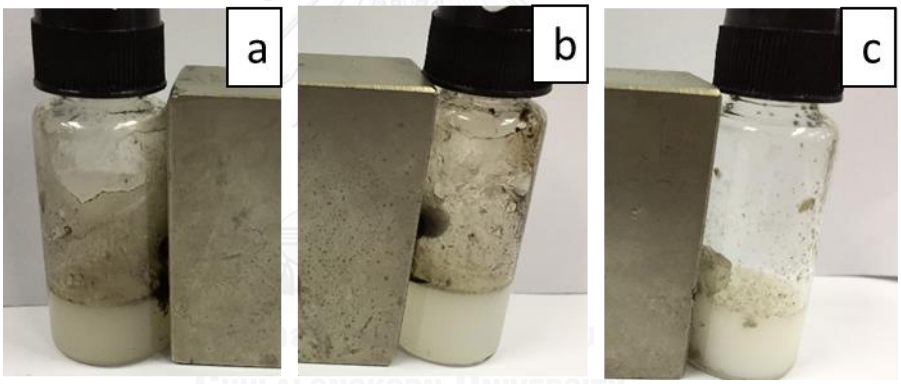

Figure A12 *Images of reused $ZnFe_2O_4$ in the order of (a) 1st, (b) 2nd, and (c) 3rd run with external magnet*

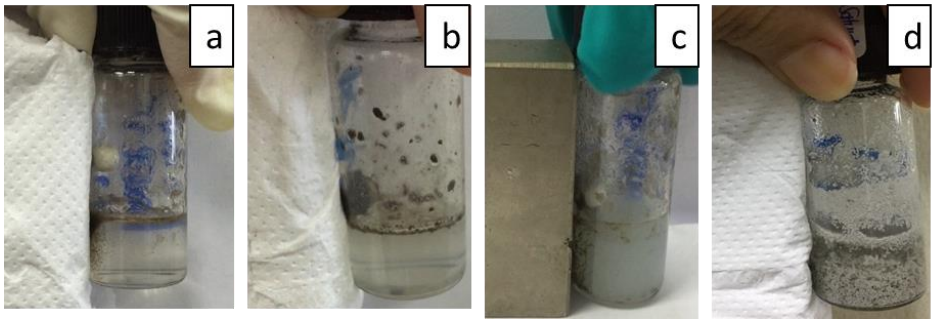

Figure A13 *Images of reused $CuFe_2O_4$ in the order of (a) 1st run, (b) 2nd run, (c) 3rd run, and (d) 4th run with external magnet*

VITA

Ms. Haruethai Kongcharoen was born on October 1, 1992 in Chonburi, Thailand. She graduated in Bachelor's Degree under supervision of Dr. Numpon Insin from Department of Chemistry, Faculty of Science in Chulalongkorn University in 2014 and continuously pursued her Master's Degree in the same group. Furthermore, she was offered the scholarships from the Graduate School, Chulalongkorn University to commemorate the 72nd anniversary of his Majesty King Bhumibala Aduladeja for supporting the graduate study and also became a member of Materials Chemistry and Catalysis Research Unit since she was undergraduate student.

On 2-3 February 2017, she participated in the 11th Pure and Applied Chemistry International Conference 2017 (PACCON 2017) in the title of "SYNTHESES OF MONODISPERSE METAL-FERRITE NANOPARTICLES AND THEIR CATALYTIC ACTIVITY IN OXIDATIVE COUPLING OF THIOLS" by poster presentation.

Email address: Haruethai.ying@gmail.com